AD-A114 809 ROCKWELL INTERNATIONAL THOUSAND OAKS CA SCIENCE CENTER F/6 11/2
STRENGTHENING AND STRENGTH UNIFORMITY OF STRUCTURAL CERAMICS.(U)
MAR 82 F F LANGE F49620-81-C-0036
UNCLASSIFIED SC5295.1AR AFOSR-TR-82-0389 NL

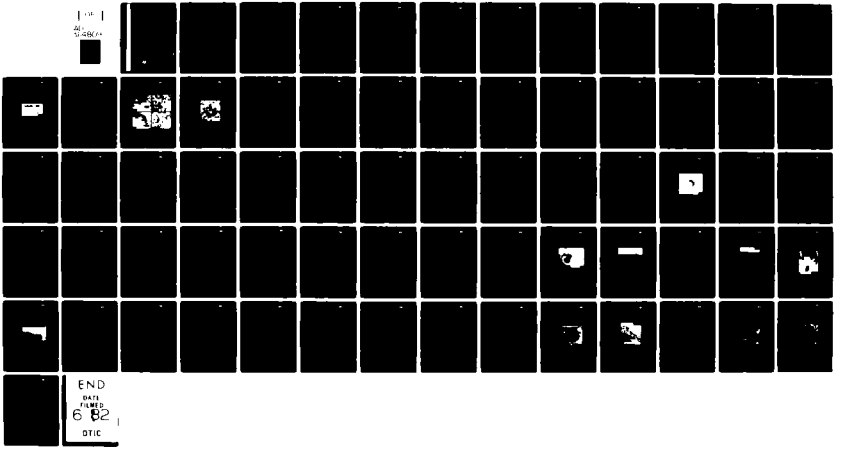

END
DATE FILMED
6 82
DTIC

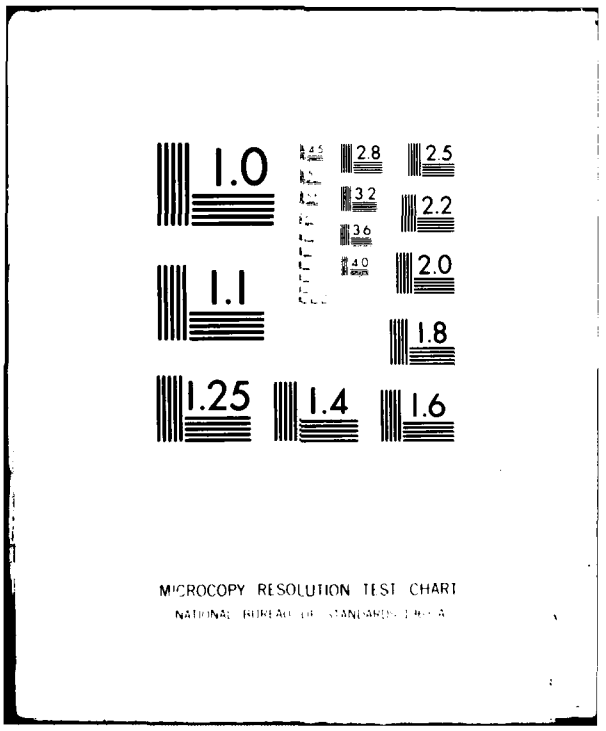
1.0
1.1
1.25
1.4
1.6
1.8
2.0
2.2
2.5
2.8
3.2
3.6
4.0
MICROCOPY RESOLUTION TEST CHART

F.F. Lange

AFOSR-TR- 82-0389

12

SC5295.1AR

Copy No. 10

SC5295.1AR

AD A114809

STRENGTHENING AND STRENGTH UNIFORMITY OF STRUCTURAL CERAMICS

ANNUAL REPORT FOR THE PERIOD
February 1, 1981 through January 31, 1982

CONTRACT NO. F49620-81-C-0036

Prepared for

Air Force Office of Scientific Research
Directorate of Electronic and Material Sciences
Building 410
Bolling Air Force Base, DC 20332

F.F. Lange
Principal Investigator

MARCH 1982

Approved for public release; distribution unlimited

Rockwell International
Science Center

UNCLASSIFIED

SECURITY CLASSIFICATION OF THIS PAGE (When Data Entered)

REPORT DOCUMENTATION PAGE	READ INSTRUCTIONS BEFORE COMPLETING FORM
1. REPORT NUMBER: AFOSR-TR- 82-0389 / 2. GOVT ACCESSION NO. AD-A114 869	3. RECIPIENT'S CATALOG NUMBER
4. TITLE (and Subtitle): STRENGTHENING AND STRENGTH UNIFORMITY OF STRUCTURAL CERAMICS	5. TYPE OF REPORT & PERIOD COVERED: Annual Report for Period 02/01/81 through 01/31/82
	6. PERFORMING ORG. REPORT NUMBER: SC5295.1AR
7. AUTHOR(s): F.F. Lange	8. CONTRACT OR GRANT NUMBER(s): F49620-81-C-0036
9. PERFORMING ORGANIZATION NAME AND ADDRESS: Rockwell International Science Center, 1049 Camino Dos Rios, Thousand Oaks, California 91360	10. PROGRAM ELEMENT, PROJECT, TASK AREA & WORK UNIT NUMBERS: 2306/A2 61102F
11. CONTROLLING OFFICE NAME AND ADDRESS: Air Force Office of Scientific Research/NE, Directorate of Electronic and Material Science, Building 410, Bolling Air Force Base, DC 20332	12. REPORT DATE: March 1982
	13. NUMBER OF PAGES: 66
14. MONITORING AGENCY NAME & ADDRESS(if different from Controlling Office)	15. SECURITY CLASS. (of this report): UNCLASSIFIED
	15a. DECLASSIFICATION/DOWNGRADING SCHEDULE

16. DISTRIBUTION STATEMENT (of this Report)

Approved for public release; distribution unlimited.

17. DISTRIBUTION STATEMENT (of the abstract entered in Block 20, if different from Report)

18. SUPPLEMENTARY NOTES

19. KEY WORDS (Continue on reverse side if necessary and identify by block number)

Agglomerates, Fracture Differential Sintering, Power Consolidation Al_2O_3, ZrO_2

20. ABSTRACT (Continue on reverse side if necessary and identify by block number)

Appendix I: Strengths of sintered Al_2O_3/ZrO_2 composites are much lower than hot-pressed composites due to large flaws associated with the sintering process. Fractography has shown that crack-like internal surfaces are at the fracture origins of the sintered materials. It is hypothesized that the crack-like internal surfaces are developed due to differential sintering of agglomerates relative to their surrounding powder compact. HIP treatment of the sintered composites quickly eliminated the crack-like internal surface.

DD FORM 1 JAN 73 1473 EDITION OF 1 NOV 65 IS OBSOLETE

UNCLASSIFIED

SECURITY CLASSIFICATION OF THIS PAGE (When Data Entered)

Flaws responsible for fracture of the HIP treated composites were low density regions that are not as quickly eliminated.

Appendix II: Effects of differential sintering kinetics due to differential green density were studied by fabricating agglomerate-powder matrix specimens from two different Al_2O_3/ZrO_2 (30 v/o) powders and subjecting them to a cyclic sintering schedule to allow intermittent observations. Low green density compacts sintered at a greater rate than high density compacts, although high green density compacts reached end-point densities first. Specimens containing low green density agglomerates produced circumferential crack-like voids at the agglomerate/matrix interface. Agglomerates with a higher green density than the matrix were subjected to compressive strains by the matrix to produce agglomerate mobility when the resulting stress field was non-symmetric. Such agglomerates also produced a variety of crack-like separations. Implications regarding sintering kinetics and end-point densities are discussed. Implications regarding strength to sintered bodies are obvious, viz: strength can be proportional to the square-root of the agglomerate size.

Appendix III: Large ZrO_2 hard agglomerates remained in an Al_2O_3/ZrO_2 composite suspension after inefficient ball milling. The ZrO_2 agglomerates shrank away from the consolidated Al_2O_3/ZrO_2 powder matrix during sintering, producing crack-like voids which were responsible for strength degradation.

PROGRAM SUMMARY

The first year effort of this program has produced a major advance in uncovering the processing steps that result in strength degrading flaws in sintered ceramics. This advance was initiated when a dye-penetrant was used to examine sintered materials (namely, a series of tough Al_2O_3/ZrO_2 composites), (see Fig. 2, Appendix 1). Our observations suggested that the small volume elements that absorbed the dye were low density regions and that these low density regions were the strength degrading flaws which only allowed the sintered material to achieve 1/2 the strength that hot-pressed materials of the same composition achieve (Fig. 1, Appendix 1). Although this initial conclusion was later shown to be wrong, it did point a direction to uncover the real processing flaw responsible for strength degradation.

As detailed in Appendix 1, successful attempts were made to eliminate the low density volume elements by HIPing (Hot-Isostatic Pressing), and strength increased as expected. But when the fracture origins were examined, only low density porous regions were observed in the HIPed materials. In the sintered materials, the fracture origins were not low density regions as initially expected, but internal, sintered surfaces as shown in Fig. 3 of Appendix 1. The question then arose, how can an internal surface form during sintering? (Internal, crack-like surfaces pre-existing in the unsintered powder compact were ruled out, since all specimens were isostatically cold pressed prior to sintering.) The morphologies of the material bounding the internal surfaces (Fig. 3, Appendix 1) strongly suggested that large agglomerates in the powder compact shrank away from the surrounding powder matrix during sintering to produce a crack-like void. It was further postulated that HIPing simply closed these crack-like voids and thus resulted in a strengthening. Further, other agglomerates did not sinter as rapidly as the matrix to produce the low density regions in the sintered materials evident by the absorption of the dye. From a fracture standpoint, these low density regions were not as detrimental as the large crack-like voids. HIPing quickly eliminated the crack-like voids, but not the porous regions which now became the predominant strength reducing flaws in the HIPed materials.

The hypothesis that agglomerates in a powder compact lead to crack-like voids directed the second and major part of this year's effort detailed in Appendix 2. It was reasoned that the major differences between agglomerates and between agglomerates and their surrounding powder matrix were green density differentials. A simple analysis showed that the differential strain produced between an agglomerate of density (ρ_{oa}) and its matrix (ρ_{om}) would always be either compressive or tensile:

$$\Delta\varepsilon = \varepsilon_m - \varepsilon_a = \left(\frac{\rho_{oa}}{\rho_a}\right)^{1/3} - \left(\frac{\rho_{om}}{\rho_m}\right)^{1/3}$$

since $\rho_a \rightarrow \rho_m \rightarrow \rho_t$ (the theoretical, or end-point, density achieved by sintering).

Much effort was directed to produce specimens with single, large agglomerates with well defined differential green densities (Fig. 2, Appendix 2). A new technique was also developed to impress an orthogonal grid on the specimen's surface to measure sintering strain and thus density of the agglomerate and its surrounding matrix and to observe the perturbation of the matrix strain due to differential sintering. The effect of phase transformation on differential strain was also investigated.

This effort can be summarized with the following pertinent results:

1) It was shown that densification rate is inversely proportional to green density (Fig. 5, Appendix 2).

2) Agglomerates with a lower green density than their matrix will densify more rapidly, separating from the matrix to produce a crack-like void (Fig. 14, Appendix 2), thus confirming the hypothesis in Appendix 1.

3) Lower density matrices densify more rapidly and place the agglomerate under compressional strain. This "shrink fit" of the matrix around the agglomerate perturbs the matrix's strain field (Figs. 8 and 9, Appendix 2).

4) Agglomerates placed under compressional strain (and stress) become mobile when the stress field is non-symmetric, as is the case of the surface agglomerate. This causes the agglomerate to be pushed out of the surface (shown in Fig. 10, Appendix 2).

5) A variety of cracks form due to differential sintering for the case where the agglomerate is under compression (Figs. 14-18, Appendix 2).

6) Differential strains can also be produced by phase transformations (e.g., the $\gamma \rightarrow \alpha\text{-}Al_2O_3$ and $m \rightarrow ZrO_2$ structural transformation).

These observations not only have great significance concerning strength, but also concerning densification itself. First, it can be seen that agglomerates produce cracks due to differential sintering. Since strength is inversely proportional to the square-root of the crack size, strength will be inversely proportional to the square-root of the agglomerate size. Namely, processing routes that minimize the size of agglomerates must be found. Second, the crack-like voids produced by differential sintering limit the end-point density that can be acheived by sintering, and agglomerate mobility produces long range mass movement that can not be achieved by diffusion.

The third piece of work demonstrated how improper milling conditions can lead to strength degrading agglomerates in two-phase composite ceramics as detailed in Appendix 3. Large, hard ZrO_2 agglomerates in the ZrO_2 powder were not broken apart when they were milled together with the Al_2O_3 powder. These large agglomerates produce large crack-like voids due to differential sintering (Figs. 1 and 2, Appendix 3) and thus significantly reduce the potential strength of this tough ceramic.

LIST OF PUBLICATIONS THAT WILL RESULT FROM CURRENT AFOSR PROGRAM

1. F.F. Lange, "Processing Realted Fracture Origins; Part 1, Observations in Sintered and HIP Treated Al_2O_3/ZrO_2 Compositions."

2. F.F. Lange and M. Metcalf, "Processing Related Fracture Origins: Part 2, Agglomerate Mobility and Crack-Like Internal Surfaces Caused by Differential Sintering."

3. F.F. Lange and I.A. Aksay, "Processing Related Fracture Origins: Part 3, Differential Sintering of ZrO_2 Agglomerates in Al_2O_3/ZrO_2 Composites."

PERSONNEL INVOLVED

F.F. Lange
B.I. Davis
M. Metcalf
I.A.Aksay*

OTHER INTERACTIONS (ORAL PRESENTATIONS)

1. Portions of Appendices 1 and 2, Rutgers University, December 18, 1981.

2. Portions of Appendix 2, UCLA Short Course, February 4, 1982.

*Associated Prof., Materials Science and Engineering Dept. UCLA.

APPENDIX I
PROCESSING RELATED FRACTURE ORIGINS: PART 1, OBSERVATIONS IN SINTERED AND HIP TREATED Al_2O_3/ZrO_2 Composites

F. F. Lange
Structural Ceramics Group

Abstract

Strengths of sintered Al_2O_3/ZrO_2 composites are much lower than hot-pressed composites due to large flaws associated with the sintering process. Fractography has shown that crack-like internal surfaces are at the fracture origins of the sintered materials. It is hypothesized that the crack-like internal surfaces are developed due to differential sintering of agglomerates relative to their surrounding powder compact. HIP treatment of the sintered composites quickly eliminated the crack-like internal surface. Flaws responsible for fracture of the HIP treated composites were low density regions that are not as quickly eliminated.

Introduction

While attempting to sinter Al_2O_3/ZrO_2 composite powders to achieve strengths comparable to those obtained by hot-pressing, it was noticed that a dye-penetrant revealed large (50-500 μm), irregular, low density regions on cut surfaces of dense (> 98% of theoretical) materials. Since the strength of these sintered materials was < 1/2 that obtained by hot-pressing, it was first concluded that the large, low-density regions were the strength degrading flaws. Attempts to reduce the size of these low density regions by improved powder processing did result in moderate strengthening. In an attempt to eliminate the low density regions, the author used the HIP (hot-isostatic-pressing) treatment suggested by Engle and Hubner[1] and initiated a systematic study relating strength to processing variables. As will be shown below, the low density regions were only of secondary importance and the crack-like internal surfaces

produced by differential sintering kinetics were primarily responsible for the lower strength obtained by sintering powders consolidated by dry pressing.

Experimental

Materials in the Al_2O_3/ZrO_2 system containing 30 v/o, 40 v/o and 50 v/o of ZrO_2 (+ 2 m/o Y_2O_3) were chosen for study. As discussed elsewhere, tetragonal ZrO_2 is a significant toughening agent.[2] Y_2O_3, which partitions to the ZrO_2 during sintering, helps retain the tetragonal ZrO_2 structure in its constrained state for grain sizes that are obtained during densification at 1600°C.[2]

Composite powders were prepared by milling the appropriate amounts of sub-micron size Al_2O_3,* ZrO_2** and $Y(NO_3)_3$*** powders in alcohol. The mixed composite powders were dried by rotary distillation, calcined at 600°C to decompose the $Y(NO_3)_3$ to Y_2O_3, and again ground prior to consolidation. Square plates (~ 5 cm × 5 cm) were uniaxially pressed (~ 30 MPa) from each composite powder and then isostatically pressed (350 MPa) prior to sintering at 1600°C/2 hrs in air. As shown in Table I, densities > 98% of theoretical were achieved.

One half of a plate of each of the sintered materials was cut into bar specimens (~ 0.3 × 0.6 × 3.5 cm) for 4-pt flexural strength determinations (inner span: 1.27 cm; outerspan: 2.54 cm). The other half was HIPed in argon at 1500°C/100 MPa/1/2 hr and then cut into bar specimens. A second plate of each sintered material was HIPed at 1500°C/200 MPa/1 hr and cut into specimens. All bar specimens were diamond ground in the same manner to preclude effects of differential surface preparation on the strength results.

*Alcoa A-16
**Zircor Corp.
***Research Chemical Inc.

Table I

Al_2O_3/ZrO_2 Composite Properties

Vol % ZrO_2*	Sintered Density (% theoretical)**	HIP Conditions	HIP Density (% theoretical)	Average Strength (MPA)***
98.1	-	-	558 (5)	
30	98.1	1500°C/100 MPa/0.5 hr	99.8	838 (5)
98.4	1500°C/200 MPa/1 hr		100.0	869 (8)
98.2	-	-	607 (5)	
40	98.2	1500°C/100 MPa/0.5 hr	99.5	867 (5)
98.6	1500°C/200 MPa/1 hr		100.0	913 (8)
98.0	-	-	613 (5)	
50	98.0	1500°C/100 MPa/0.5 hr	99.4	855 (5)
99.2	1500°C/200 MPa/1 hr		100.0	1000 (8)

*ZrO_2 + 3 mole % Y_2O_3

**$\rho_{Al_2O_3}$ = 3.98 g•cm^{-3}; ρ_{ZrO_2} = 6.08 g•gm^{-3}

***Number of specimens in brackets.

Observations

As reported in Table I and Fig. 1, the strength of sintered materials could be significantly increased with a HIP treatment. But it should be noted that the HIP treated material was still weaker than the hot-pressed material. Dye-penetrant observations showed that HIPing did reduce the size and number of the low density regions prevalent in the sintered materials. This is illustrated in Fig. 2 for a set of Al_2O_3/30 v/o ZrO_2 materials; the HIP treatment at 1500°C/200 MPa/1 hr appeared to eliminate the low density regions.

Fractography was most revealing. Fracture origins of sintered materials were easily located, since fragmentation was not prevalent at lower strengths. Contrary to expectations, dye-penetration of the fracture surface of sintered materials showed that fracture origin was not a low density region. Low-density regions were usually observed elsewhere on the fracture surface, but

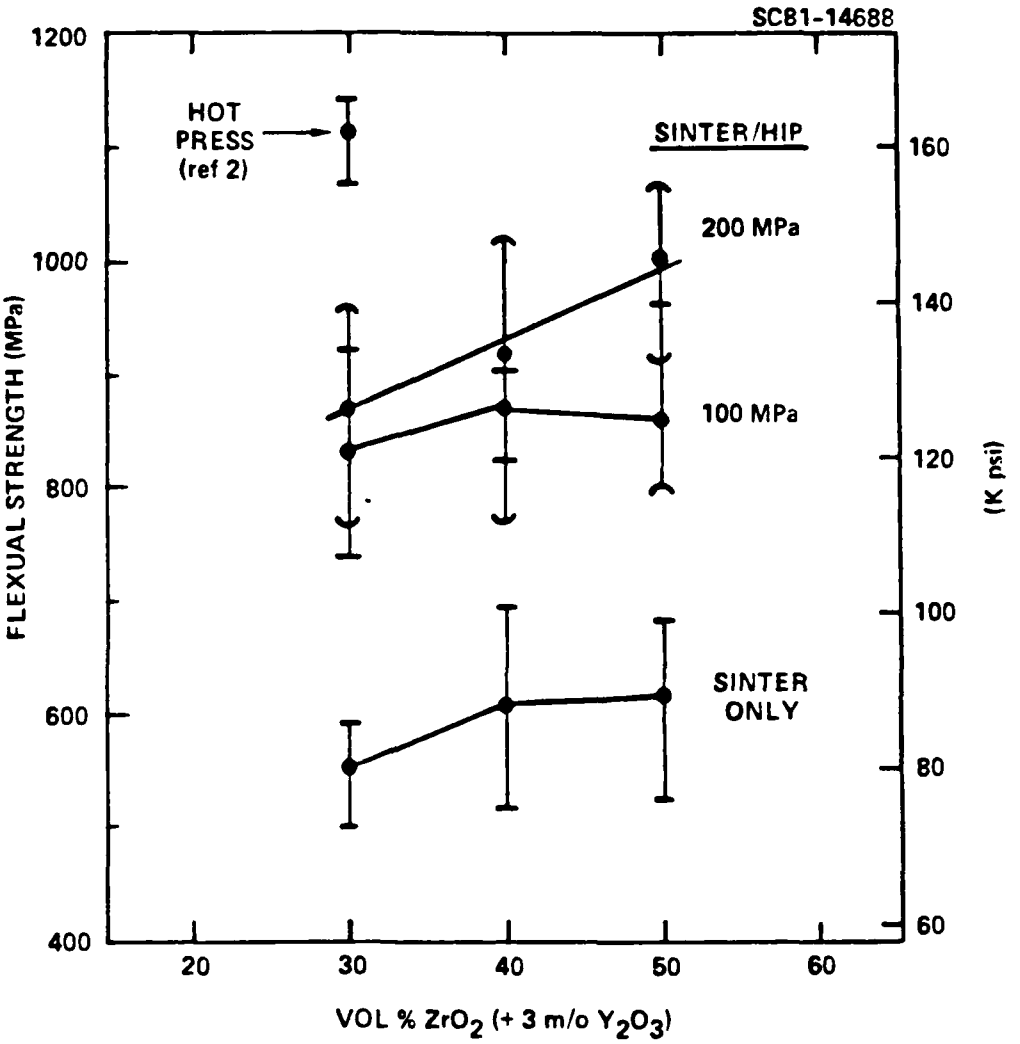

Fig. 1 Flexural strength of Al_2O_3/ZrO_2 (+ 3 m/o Y_2O_3) materials.

SC81-14687

Fig. 2 Representative dye-penetrant results (a) sintered, (b) sinter/HIP-1500°C/100 MPa/0.5 hr, and (c) sinter/HIP-1500°C/200 MPa/1 hr.

not at the fracture origin. A typical fracture origin for sintered materials is shown in Fig. 3a. Detailed analysis showed that surfaces of these irregular protrusions had the characteristics of a sintered surface (smooth grain morphologies as shown in Fig. 3b), whereas surfaces remote to the protrusion exhibited typical fracture morphologies as shown in Fig. 3d. When the surface was scanned from the center of the protrusion to a remote position, one could see a general change in surface morphology from that shown in Fig. 3b to the one shown in Fig. 3d. The frequency of cross-surface bonding increased as one traversed toward the protrusion's apparent boundary. These observations clearly showed that the surface of the protrusion was an internal surface occasionally bonded to the opposite internal surface with a few grains.

Figure 3c illustrates the morphology of a less typical fracture origin for the sintered materials. Here, the protrusion is undercut by another internal surface, strongly suggesting that the protrusion is part of an agglomerated mass of grains which had separated from the surrounding material during densification.

The morphology of fracture origins for the HIP treated materials was quite different. Although fragmentation prevented the examination of all origins, those examined appeared to be irregular-shaped pores as shown in Fig. 4. Crack-like internal surfaces were never observed.

Discussion

Contrary to initial reasoning, fractography revealed that sintered specimens failed from large, crack-like internal surfaces which were eliminated by a HIP treatment. HIPed materials failed from small irregular-shaped pores which may be remnants of the large porous regions observed in the sintered materials.

The formation of crack-like internal surfaces due to the differential sintering kinetics of powder agglomerates relative to their surrounding powder matrix has been reported by Reeve[3] and Vasidos and Rhodes.[4] Fractography evidence suggests a similar phenomenon for the formation of crack-like internal surfaces observed in the present study. Although powder characteristics such as

SC81-14689

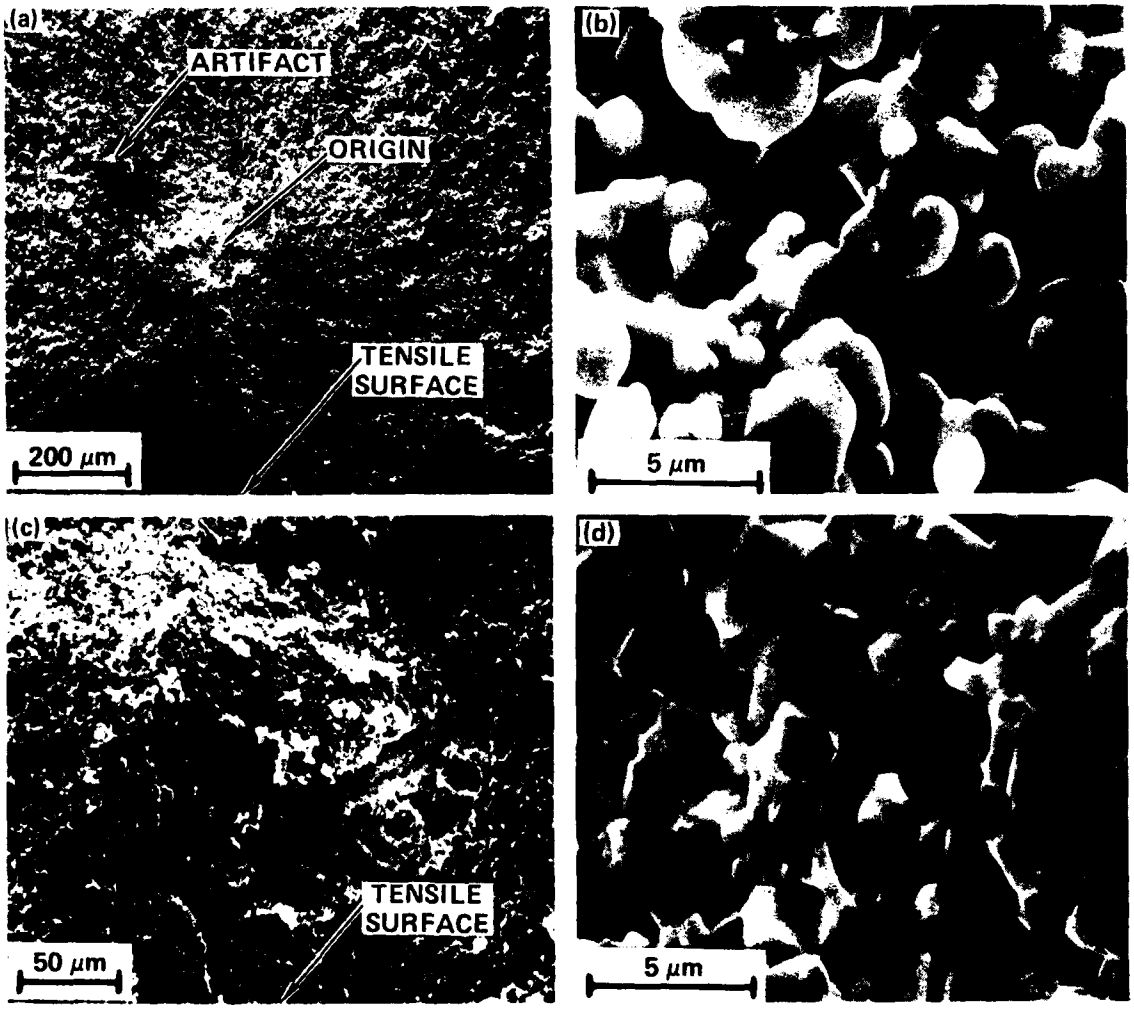

Fig. 3 (a) and (c) fracture origin of sintered material; (b) internal surface morphology; (d) fracture surface remote from protrusion.

SC81-14686

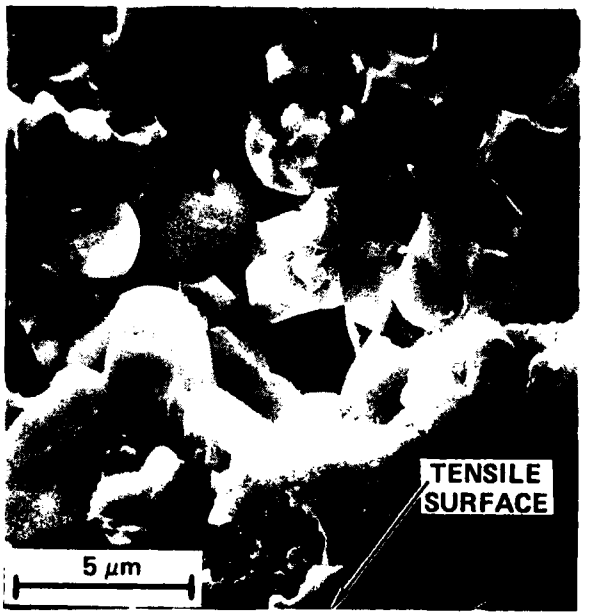

Fig. 4 Pore at origin of HIP treated material.

particle size and chemistry are most widely recognized factors controlling densification kinetics, Bruch[5] has shown that the initial green density of the powder compact has a pronounced effect. Bruch pointed out that very low green densities result in sub-normal sintering kinetics, i.e., a region where the time exponent is much smaller than expected. He also showed that within the regime of normal sintering kinetics (where the time exponent is independent of green density), green density governs the magnitude of the sintering rate coefficient. When his results are applied to agglomerated powders, one can see that differential green density will produce differential sintering kinetics.

It is obvious to conclude that agglomerates within powders can have different green densities. Agglomerates with very low green densities will exhibit sub-normal sintering kinetics to produce porous regions detectable by dye-penetration. Denser agglomerates with fast sintering kinetics will separate from their surrounding powder matrix to produce crack-like internal surfaces. Both of these situations have been simulated by the author by incorporating large spherical agglomerates into powder matrices with different green densities. As reported elsewhere,[6] not only do differential sintering rates produced by differential densities lead to the formation of internal surfaces, but they also lead to stresses that can cause agglomerate mobility during densification.

In conclusion, it has been shown that crack-like internal surfaces produced by differential sintering rates can be quickly eliminated by a HIP treatment, whereas large porous regions were reduced at the slower rate. Fractography revealed that the crack-like internal surfaces were responsible for the lower strengths of sintered materials, whereas pores limited the strength of HIP treated sintered materials. Methods of consolidating non-agglomerated powders should be sought to optimize the microstructural uniformity and strength of sintered materials.

Acknowledgments

This work was supported by the Air Force Office of Scientific Research under Contract No. F49620-81-0036.

References

1. V. Engle and H. Hubner, "Strength Improvement of Cemented Carbides by Hot Isostatic Pressing," J. Mat. Sc. 13, 2003-2013 (1978).

2. F.F. Lange, "Transformation Toughening, Parts 1, 2, 3, 4, 5," J. Mat. Sci. (in press).

3. K.D. Reeve, "Non-Uniform Shrinkage in Sintering," Bul. Amer. Ceram. Soc. 42 [8] 452 (1963).

4. T. Vasidos and W. Rhodes, pp. 137-172 in Ultrafine-Grain Ceramics. Ed. by J.J. Burke, N.L. Reed and V. Weiss; Syracuse University, N.Y. 1970.

5. C.A. Bruch, "Sintering Kinetics for the High Density Alumina Process," Bull. Amer. Ceram. Soc. 41 [12] 799-807 (1962).

6. F.F. Lange and M. Metcalf "Part 1, Agglomerate Mobility and Crack-Like Internal Surfaces Caused by Differential Sintering," (to be published).

SC5295.1AR

APPENDIX II
PROCESSING RELATED FRACTURED ORIGINS: PART 2, AGGLOMERATE MOBILITY AND CRACK-LIKE INTERNAL SURFACES CAUSED BY DIFFERENTIAL SINTERING

F.F. Lange and M. Metcalf

Structural Ceramics Group
Rockwell International Science Center

Abstract

Effects of differential sintering kinetics due to differential green density were studied by fabricating agglomerate-powder matrix specimens from two different Al_2O_3/ZrO_2 (30 v/o) powders and subjecting them to a cyclic sintering schedule to allow intermittent observations. Low green density compacts sintered at a greater rate than high density compacts, although high green density compacts reached end-point densities first. Specimens containing low green density agglomerates produced circumferential crack-like voids at the agglomerate/matrix interface. Agglomerates with a higher green density than the matrix were subjected to compressive strains by the matrix to produce agglomerate mobility when the resulting stress field was non-symmetric. Such agglomerates also produced a variety of crack-like separations. Implications regarding sintering kinetics and end-point densities are discussed. Implications regarding strength of sintered bodies are obvious, viz. strength can be proportional to the square-root of the agglomerate size.

1. Introduction

Recent work has shown that internal, crack-like surfaces are located at the fracture origins of sintered materials in the Al_2O_3/ZrO_2 composite system.[1] These internal surfaces are responsible for the much lower strengths that can be achieved by cold powder compaction and sintering relative to either HIP-treated sintered materials or hot-pressed materials. Fractography observations strongly suggest that the internal surfaces are produced by the differential sintering of large agglomerates relative to their surroundings in the powder compact.

Agglomerated particles are common to all current powders. Agglomerates can be formed both during powder manufacture (decomposition/calcination) and powder processing prior to consolidation and sintering (e.g., dry-milling, spray-drying, etc.). Sedimentation results suggest that agglomerates found in milled powders can be small (< 10 μm), but strongly bonded together. On the other hand, agglomerates formed during powder processing can be large (> 50 μm), but are easily broken apart by the use of surfactants in liquid systems. Powders must be consolidated prior to sintering. Many consolidation routes involve cold-pressing dry powders (e.g., isostatic pressing). Although the applied pressure may break up many of the soft agglomerates and some of the hard agglomerates, experience suggests that both types can remain after the pressure-consolidation step. Consolidation of a dispersed liquid system by filtration (e.g., slip casting), on the other hand, if done properly, should result in a powder compact with only the smaller, hard agglomerates. Thus, one can conclude that consolidated compacts are made up of agglomerates surrounded by a matrix of particles (or smaller agglomerates). Their size distribution, volume content, and type (hard or soft) will depend on the routes used to 1) make the powder, 2) prepare the powder for consolidation, and 3) consolidate the powder for sintering.

Agglomerates within the powder compact might be expected to differ from one another and from their surrounding matrix with respect to density, average particle size, and chemistry (e.g., for the case of two-phase powders). Although all of these factors are known to govern sintering kinetics, effort was directed to the study of differential sintering due to differential density since the larger agglomerates, which would be expected to produce the larger

internal surfaces due to differential sintering, might differ most with respect to green density.

The object of the experimental program was to simulate an agglomerate/powder matrix system and to characterize the phenomena associated with its differential sintering. As shown below, not only are a variety of internal, crack-like surfaces produced under different conditions, but also non-uniform stresses arising during densification can cause agglomerate mobility. Before reporting the experiments and results leading to these observations, the following sections discuss the expected strains due to differential densification and the expected effect that green density has on sintering kinetics.

2. Differential Strain Between Agglomerates and Surrounding Powder Compact

The relation between the linear strain, ε, [$\varepsilon = (\ell-\ell_o/\ell_o)$, ℓ_o = initial dimension prior to sintering, ℓ = dimension after some sintering] and density, ρ , is given by

$$\rho = \frac{\rho_o}{(1-\varepsilon)^3} \quad , \tag{1}$$

where ρ_o is the initial (green) density of the powder compact. Assuming that the densification of the agglomerate does not influence the densification of its surrounding powder matrix, the differential strain developed after some sintering between an isolated agglomerate (subscript a) and the matrix (subscript m) is

$$\Delta\varepsilon = \varepsilon_m - \varepsilon_a = \left(\frac{\rho_{oa}}{\rho_a}\right)^{1/3} - \left(\frac{\rho_{om}}{\rho_m}\right)^{1/3} \quad , \tag{2}$$

where ρ_{oa}, ρ_{om} are the respective green densities of the agglomerate and matrix. Examination of Eq. (2) shows that $\Delta\varepsilon$ is only zero when $\rho_m/\rho_a = \rho_{om}/\rho_{oa}$. Since $\rho_a \to \rho_m \to \rho_t$ (the theoretical density), viz $\rho_m/\rho_a \to 1$, as sintering proceeds, one can conclude that differential strain will develop during sintering for all cases where $\rho_{om}/\rho_{oa} \neq 1$, regardless of the dependence of densification rate on

green density.

The type of differential strain (compressive or tensile) will depend on whether the agglomerate densifies faster or slower than the matrix or, for the unexpected case where $\dot{\rho}_a/\dot{\rho}_m = \rho_{oa}/\rho_{om}$ ($\dot{\rho}$ is the densification rate), which one reaches its end-point density first. As indicated above, only differential green density will be assumed to cause differential sintering. If other microstructural dependencies are included, e.g., particle size, then differential strains will also develop when $\rho_{om}/\rho_{oa} = 1$. One can rearrange Eq. (2) to give

$$\Delta\varepsilon = \left(\frac{\rho_{om}}{\rho_m}\right)^{1/3}\left[\left(\frac{\rho_{oa}}{\rho_{om}}\right)^{1/3}\left(\frac{\rho_a}{\rho_m}\right)^{-1/3} - 1\right] , \qquad (3)$$

which will be used in subsequent sections. Examination of Eq. (3) shows that the ratio (ρ_a/ρ_m) determines the sign of $\Delta\varepsilon$ (compressive or tensile).

The magnitude of the stress developed by the differential strain will depend on the stress-strain behavior of the agglomerate and matrix. Although this subject is beyond the scope of the present paper, one can examine bounding cases. One is where both agglomerate and matrix have a viscous response; here the stress would be proportional to the differential strain rate. The other bounding case is where both are elastic; here the stress would be proportional to the differential strain. The real situation might be expected to lie between these bounds, e.g., a viscoelastic response. The stress-strain response of both agglomerate and matrix are expected to change as their microstructures (porosity, grain size, etc.) change during densification.

Although the magnitude of the stress cannot be well defined, the stress distribution can be estimated from the analogous, well studied, inclusion problem.[3,4] If, e.g., the agglomerate densified faster than the matrix, isostatic tensile stresses would arise within a spherical-shaped agglomerate. Within the surrounding matrix, the radial stresses would be tensile and the tangential stresses would be compressive to define a state of pure shear. For this case, the tensile stresses may be relieved by the formation of a crack-like internal

surface around most of the agglomerate/matrix interface. Conversely, if the agglomerate was to densify slower than the matrix, isostatic compressive stresses would arise within the spherical agglomerate; within the surrounding matrix, the radial stresses would be compressive and the tangential stresses would be tensile, again to define a state of pure shear. For this case, the tangential tensile stresses in the matrix could be relieved by the formation of a crack-like internal surface which would radiate into the matrix from the agglomerate/matrix interface.

In both cases, the magnitude of the stress components would decrease in the matrix from its maximum value at the interface as $(r)^{-3}$, where r is the radial vector. This knowledge is useful in estimating the interactions between agglomerates, e.g., agglomerates may be considered essentially isolated from one another when their separation distance is greater than one diameter.[5]

Other analogies with the inclusion problem might also be useful, e.g., stress distributions for non-spherical agglomerates,[4] stress-intensity solutions,[6] and relations that would define critical agglomerate sizes which would not form crack-like internal surfaces.[6,7]

3. Bruch's[8] Observation: Densification Kinetics and Green Density

As part of a comprehensive study of the densification behavior of Lindy A, Al_2O_3 powder (+ 0.25 weight % MgO), Bruch[8] performed systematic "isothermal" experiments to relate sintering kinetics and green density. His study indicated two effects. First, he found that the time exponent in his empirical equation used to describe the densification rate could be used to define two regimes of sintering, viz. normal and sub-normal, as shown in Fig. 1. In the normal regime (higher green density and/or higher temperatures), the time exponent was independent of green density and temperature. Within the sub-normal regime, the magnitude of the time exponent was observed to decrease with decreasing green density and/or temperature, resulting in lower sintering kinetics relative to compacts within the normal regime (e.g., loose powders exhibit little densification).

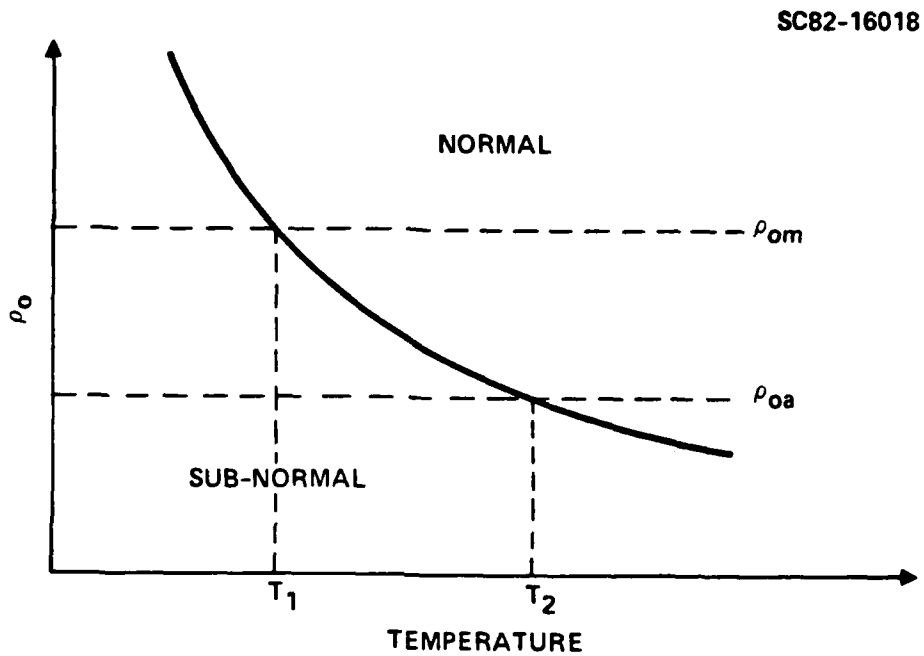

Fig. 1 Bruch's sub-normal and normal sintering regimes in green density (ρ_0)-temperature space.

Greskovich[9] has confirmed these general results with similar Al_2O_3 powders. Vasilos and Rhodes[10] observe that the sintering kinetics of ZrO_2 (stabilized with Y_2O_3) powders also exhibit sub-normal and normal sintering kinetics in a similar fashion empirically described by Bruch.

The second effect was observed by Bruch for compacts within the normal sintering regime. Here, green density had a profound effect on the rate coefficient, viz. the coefficient increased with decreasing green density. That is, within the normal regime, lower density compacts could achieve approximately the same end-point density within a given period as higher density compacts despite their initial differential green density.

Summarizing these two effects: within the sub-normal sintering regime, sintering rates increased with increasing green density, whereas, within the normal regime, sintering rates decreased with increasing green density.

If one were to use Bruch's general results and determine the density ratio (ρ_a/ρ_m) of two compacts (e.g., ρ_{oa} and ρ_{om}, in Fig. 1) as a function of temperature, one could conclude that the differential strain (see Eq. (3)) need not be of one type throughout the sintering schedule. That is, $\Delta\varepsilon$ could change from compressive to tensile (or vice versa) as each of the two compacts crossed the boundary dividing the sub-normal and normal sintering regimes as the temperature was raised (e.g., T_1 for the matrix (m) and T_2 for the agglomerate (a) as shown in Fig. 1).

4. Experimental

4.1 Powders

Two different composite Al_2O_3 + 30 v/o* ZrO_2 (+ 2 mole % Y_2O_3) powders were used for this study. One composite powder was prepared with a predominantly (~ 90%) γ-Al_2O_3 powder;** the other was prepared with α-Al_2O_3 powder.† Both composite powders contained 30 v/o monoclinic, ZrO_2.§ Previous to this work, it was demonstrated that both composite powders could be sintered to > 98% of theoretical density by heating to 1600°C for 2 hrs.[1]

Both composite powders were prepared as follows. Appropriate weight fractions of Al_2O_3, ZrO_2 and yttrium nitrate were milled together in a plastic container containing Al_2O_3 mill balls and methanol for 16 hr. The methanol was removed with a rotary distiller. The dried, composite powder was heated to 500°C for 16 hr to decompose the yttrium nitrate to Y_2O_3 and eliminate any plastic contaminants. The calcined powders were then reground dry.

4.2 Specimen Preparation

Cylindrical powder compacts containing a hemispherical surface agglomerate with a green density either higher or lower than the matrix were prepared by one of the two routes schematically shown in Fig. 2.

A majority of the specimens were prepared by the route shown in the upper portion of Fig. 2 (Route I), which first required the fabrication of spherical agglomerates. This was accomplished by isostatically pressing a powder disk that was first consolidated by uniaxial pressing at 17.5 MPa, cutting the disk into cubes, and then abrading the cubes with a high velocity air stream in a

*v/o = volume %.
**Union Carbide, Lindy B.
†ALCOA, A-16 Superground.
§Zircar, unstablized.

SC82-16013

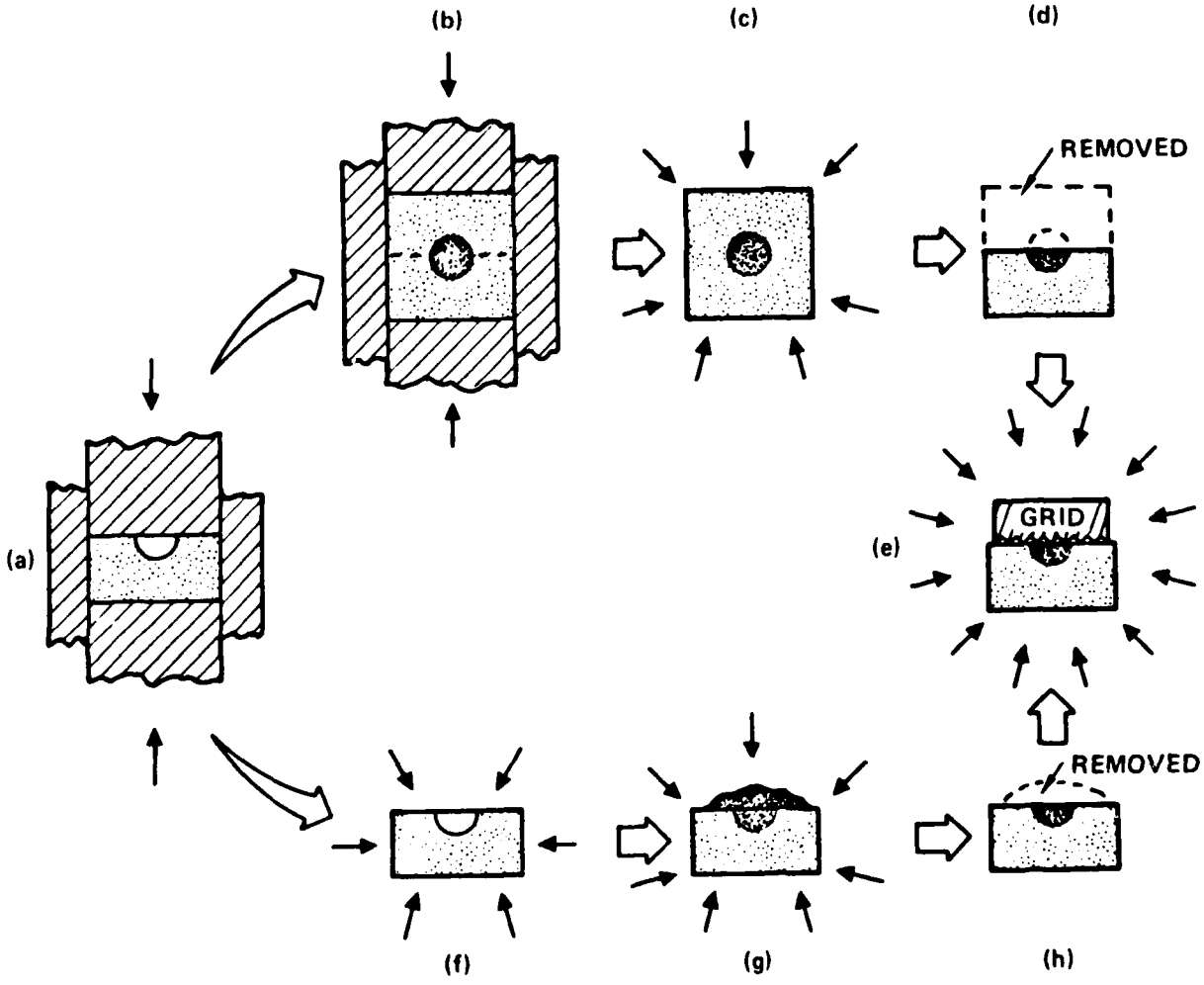

Fig. 2 Schematic illustrating the two routes to fabricate powder compacts containing a hemispherical, surface agglomerate.

cylindrical device layered with SiC paper to form spheres with diameters of ~ 0.25 cm. High- and low-density agglomerates were made in this manner from compacts isostatically pressed at 415 MPa and 70 MPa, respectively. The low density agglomerates were pre-sintered at 1200°C for 30 minutes to help prevent further densification during subsequent specimen preparation. The green density of the agglomerates were determined by weight and dimension measurements on the compact from which they were made and the sphere itself. The subsequential operations are shown in Fig. 2: a) forming a hemispherical impression in one-half of the powder, b) placing the agglomerate in the impression and uniaxially pressing (17.5 MPa) the rest of the powder to form a cylindrical compact (2.54 cm diameter), c) isostatically pressing to define the green density of the powder surrounding the agglomerate, d) sanding the compact to intercept the diameter of the agglomerate and, e) imprinting an orthogonal grid onto the specimen's surface by isostatic pressing (35 MPa).

The imprinted, orthogonal grid (formed on a metal surface by a photo-resist, etching technique developed for microelectronics) was used to measure the linear strains, due to sintering of the agglomerates and matrix, and the strain patterns developed due to differential sintering kinetics.

The second route, shown in the bottom portion of Fig. 2 (Route II), was used to ensure the formation of compacts containing low-density hemispherical agglomerates. This route avoided agglomerate pre-sintering which was necessary for fabricating the low density agglomerates in the first route. The sequence of operations consisted of a) forming a hemispherical surface cavity by uniaxial pressing (17.5 MPa), f) isostatic pressing at 420 MPa, g) filling the cavity with powder and isostatic pressing at < 420 MPa to define the green density of the agglomerate, h) removing the excess powder by careful sanding, and e) imprinting the orthogonal grid by isostatic pressing (35 MPa).

Other specimens were fabricated as described above without imprinting the orthogonal grid.

4.3 Sintering Schedules and Obvservations

A majority of the specimens were sintered with a cyclic schedule: heating to 1200°C with a 15 min hold, then cooling to room temperature, reheating to 1300°C, 15 min hold, cooling, etc., at subsequential temperatures of 1400°C, 1450°C, 1500°C, 1550°C, and 1600°C. This cyclic schedule was chosen in order to perform intermittent measurements and observations. Other specimens were simply heated to 1600°C or subjected to fewer cycles. Strain measurements showed that after a given cycle, no further densification occurred until the previous temperature and/or time was exceeded on the next cycle.

Strain due to densification was determined, from displacement of the orthogonal grid imprinted on the specimen's surface, with an optical microscope and an eye piece containing a graticule and vernier cross-hair. The agglomerate strain was determined at its center in two orthogonal directions. Matrix strain was determined near the periphery of the cylindrical specimen. The same location was used after each heating cycle. Specimen dimensions were also used to compute matrix strain and density.

After each sintering cycle, a profilometer trace was made across the specimen, intercepting the center of the agglomerate, to determine surface topography resulting from differential sintering.

After the last heating cycle, the presence and location of crack-like separations due to differential sintering were determined with a phosphorescent dye-penetrant. Specimens were also diamond-cut through the agglomerate to observe sub-surface microstructural features.

5. Results

5.1 General Densification Kinetics

Experiments not described in the previous section were designed to compare the relative densification kinetics of the two composite powders initially consolidated by isostatic pressing. This comparison was made by heating disk-shaped (isostatically pressed at 70 MPa) specimens of each powder at the same heating rate and measuring the linear shrinkage strain with a high temperature

extensometer previously used for compressive creep experiments.[11] Figure 3 reports this comparison and illustrates anomalous behavior of the γ-Al_2O_3/ZrO_2 powder, which was determined by X-ray diffraction analysis on other specimens to be caused by the $\gamma \rightarrow \alpha$ Al_2O_3 structural transformation. This transformation begins at ~ 600°C and is essentially finished at ~ 1200°C. The molar volume change associated with this transformation ($\rho_{\gamma\text{-}Al_2O_3}$ = 3.65 gm/cc vs $\rho_{\alpha\text{-}Al_2O_3}$ = 3.98 gm/cc) is, in part, responsible for this anomalous shrinkage. Morgan[12] has suggested that such transformations also aid sinterability.

The effect of the isostatic pressure on green density is shown in Fig. 4 for both composite powders. Other work[2] has shown that the γ-Al_2O_3 powder used here is highly agglomerated relative to the α-Al_2O_3 powder, suggesting a reason for the large difference in compaction behavior for the two composite powders.

Density determinations from surface shrinkage strains (Eq. (1)) were always greater than those determined from diametrical strains. Density determinations from diametrical strains were nearly identical to determinations made from specimen weight and dimension measurements. Dye penetration observations of nearly dense, sectioned specimens revealed that the material adjacent to all external sintered surfaces did not absorb the penetrant, whereas the interior readily absorbed the penetrant (shown later in Fig. 18). When these observations are combined with the surface vs diametrical strain determinations, one must conclude that the surfaces of isostatically pressed specimens densify at a greater rate than their interiors.

The effect of green density on densification rate was determined by comparing the density of one compact with another at each temperature. Figure 5 is representative of this comparison and illustrates the plot of the density ratio (ρ_ℓ/ρ_h) vs temperature for both powders, where ρ_h is the density of the compact with the highest green density and ρ_ℓ is the density of a compact within the same set. These data show that the ratio ρ_ℓ/ρ_h begins to increase and approach 1 prior to either compact achieving an end-point density. Also, since ρ_ℓ/ρ_h is always greater than $\rho_{o\ell}/\rho_{oh}$, one must conclude that within the limits of the present experiments, the lower density compact densifies at a greater

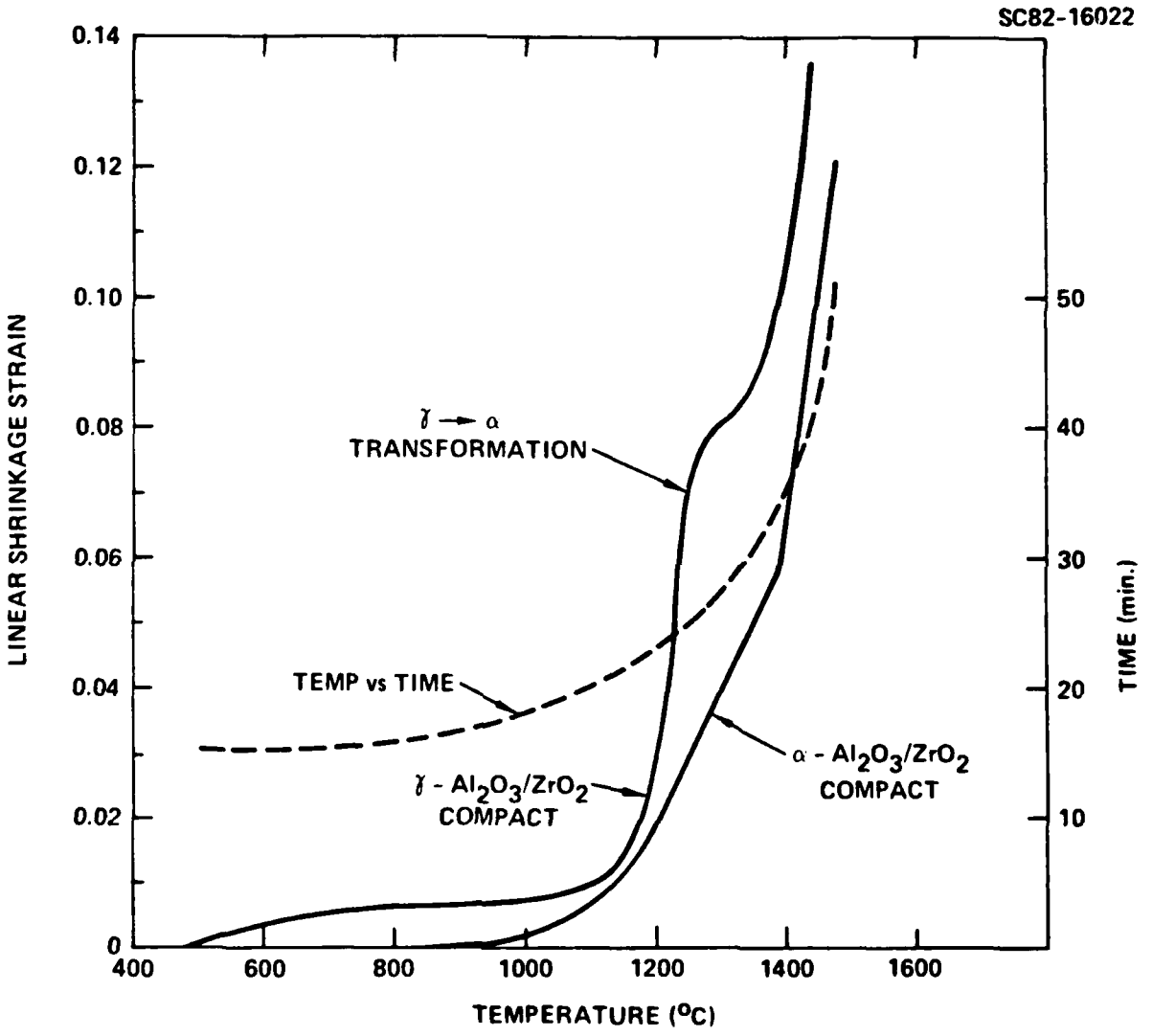

Fig. 3 Linear shrinkage strain vs temperature for the two types of powder compacts used to fabricate agglomerate/matrix powder compacts.

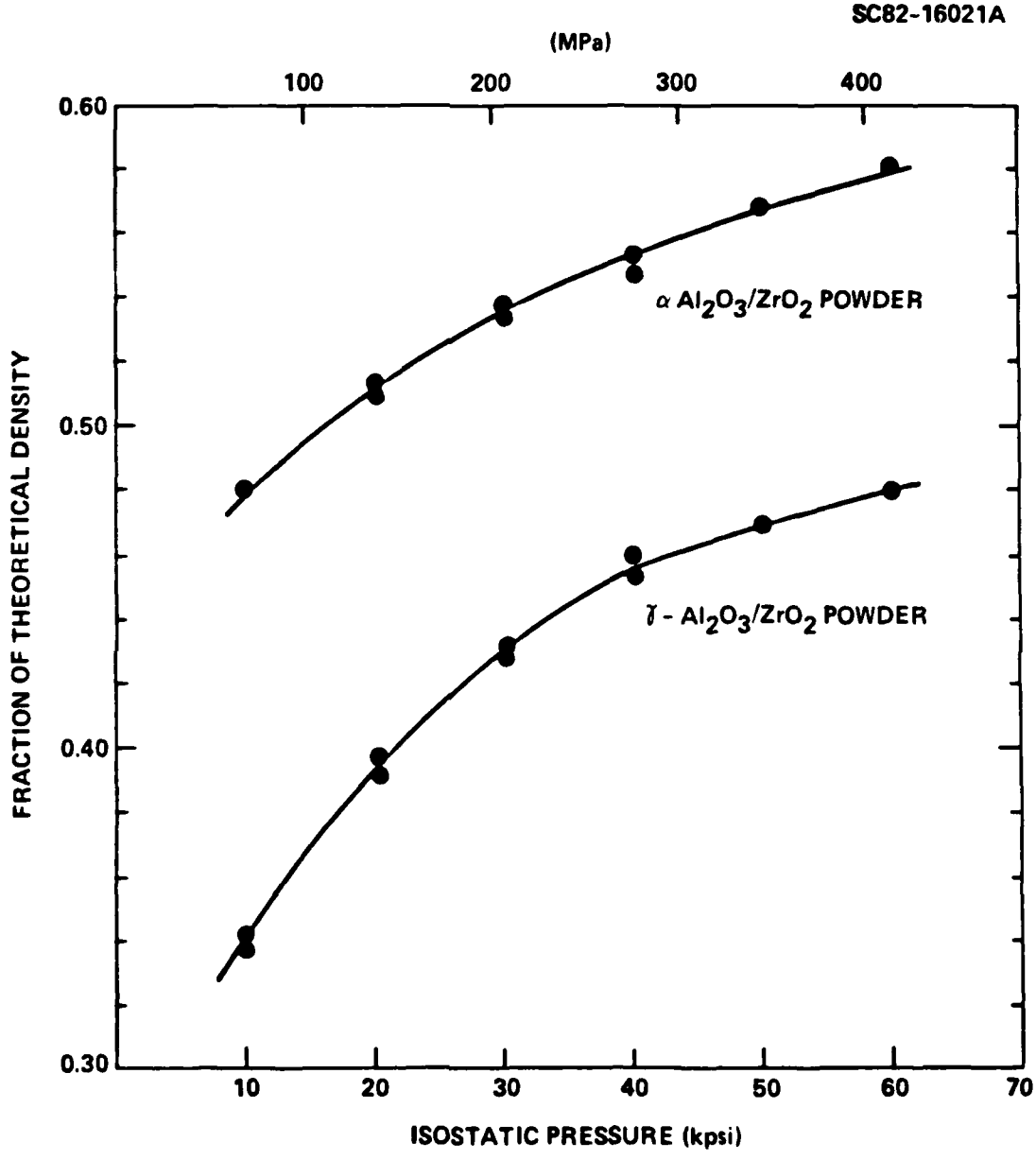

Fig. 4 Green density vs isostatic pressure.

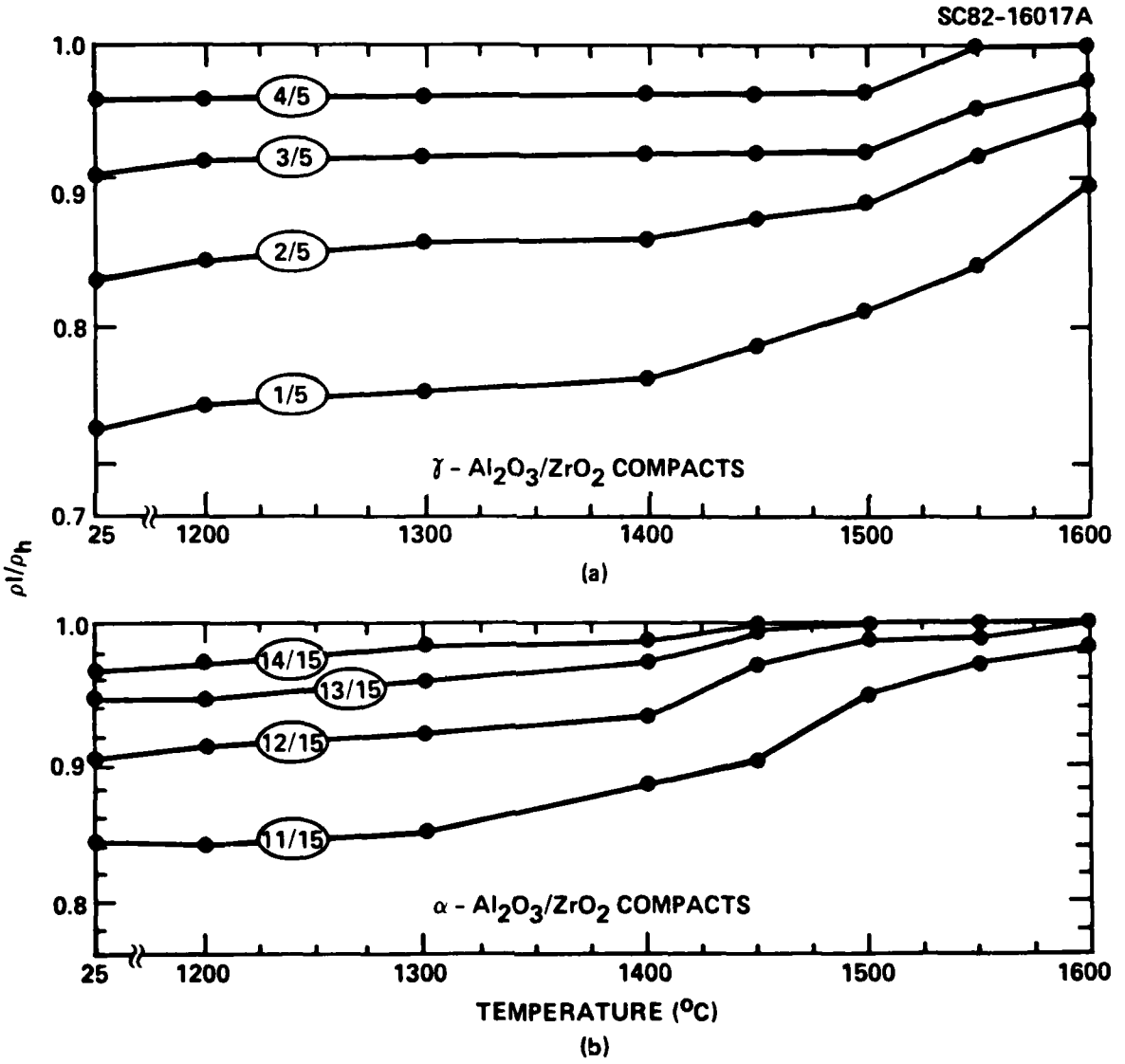

Fig. 5 Comparison of the density ratio for a series of compact sets showing that the lower density (ρ_ℓ) compact densities at a faster rate than the higher density (ρ_h) compact (viz. $\rho_\ell/\rho_h \to 1$ before either reached an end-point density).

rate than the higher density compact, in accordance with Bruch's observations for the normal sintering regime.

5.2 Agglomerate/Matrix Densification

Surface displacements of the orthogonal grid were used to compute the strain and density (Eq. (1)) of each agglomerate and their respective matrix after every sintering cycle. The ratio ρ_a/ρ_m vs temperature is shown in Figs. 6 and 7 for specimens fabricated from the two respective powders.

For specimens fabricated with high green density (HD) agglomerates and low green density (LD) matrices (specimens 6-10 and 16-19) the ratio ρ_a/ρ_m was always $> \rho_{oa}/\rho_{om}$ and tended toward unity with increasing temperature. That is, the lower density matrix exhibited a greater densification rate relative to the higher density agglomerate. The same conclusion was also reached in the above section when the densification rates of the matrices were compared with one another. Since $\rho_a/\rho_m > \rho_{oa}/\rho_{om}$, Eq. (3) shows that the matrix exerted a consistant compressive strain on the agglomerate during the entire sintering schedule.

The ratio ρ_a/ρ_m for specimens fabricated with pre-sintered (1200°C/30 min) agglomerates (1-5 and 11-15) exhibited a different behavior. Here, ρ_a/ρ_m decreased to a minimum before increasing. Surface strain measurements showed that the pre-sintered agglomerates did not undergo any densification until they were subjected to temperatures > 1200°C.

X-ray diffraction analysis of the pre-sintered γ-Al_2O_3/ZrO_2 agglomerates showed that the 1200°C/30 min pre-sintering treatment resulted in the transformation of γ-Al_2O_3 to α-Al_2O_3 consistent with the results shown in Fig. 3. In addition, the tetragonal structure of the ZrO_2 was retained on cooling to room temperature in pre-sintered agglomerates formed from both powders. The volume decreased due to the $\gamma \rightarrow \alpha$ Al_2O_3 transformation produces a linear shrinkage strain of ~ 3% and ~ 1% for the monoclinic to tetragonal ZrO_2 transformation (ZrO_2 only accounts for 30 v/o of the powder). Thus, one can conclude that the large decrease in ρ_a/ρ_m during the initial sintering cycle was caused by the phase transformations and the sintering that accompanied these

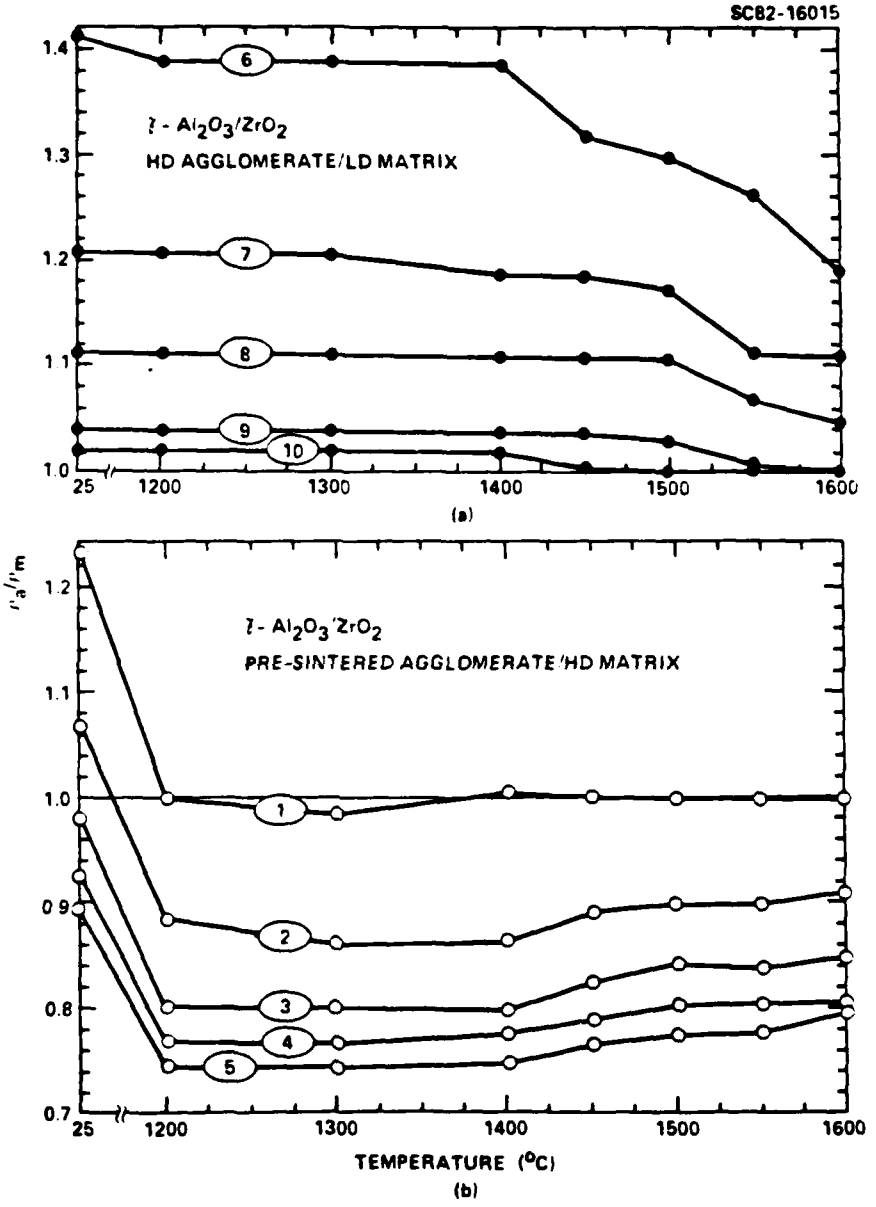

Fig. 6 Density ratio of the agglomerate (ρ_a) and its respective matrix (ρ_m) as a function of cyclic sintering temperature for specimens fabricated with the γ-Al_2O_3/ZrO_2 composite powder.

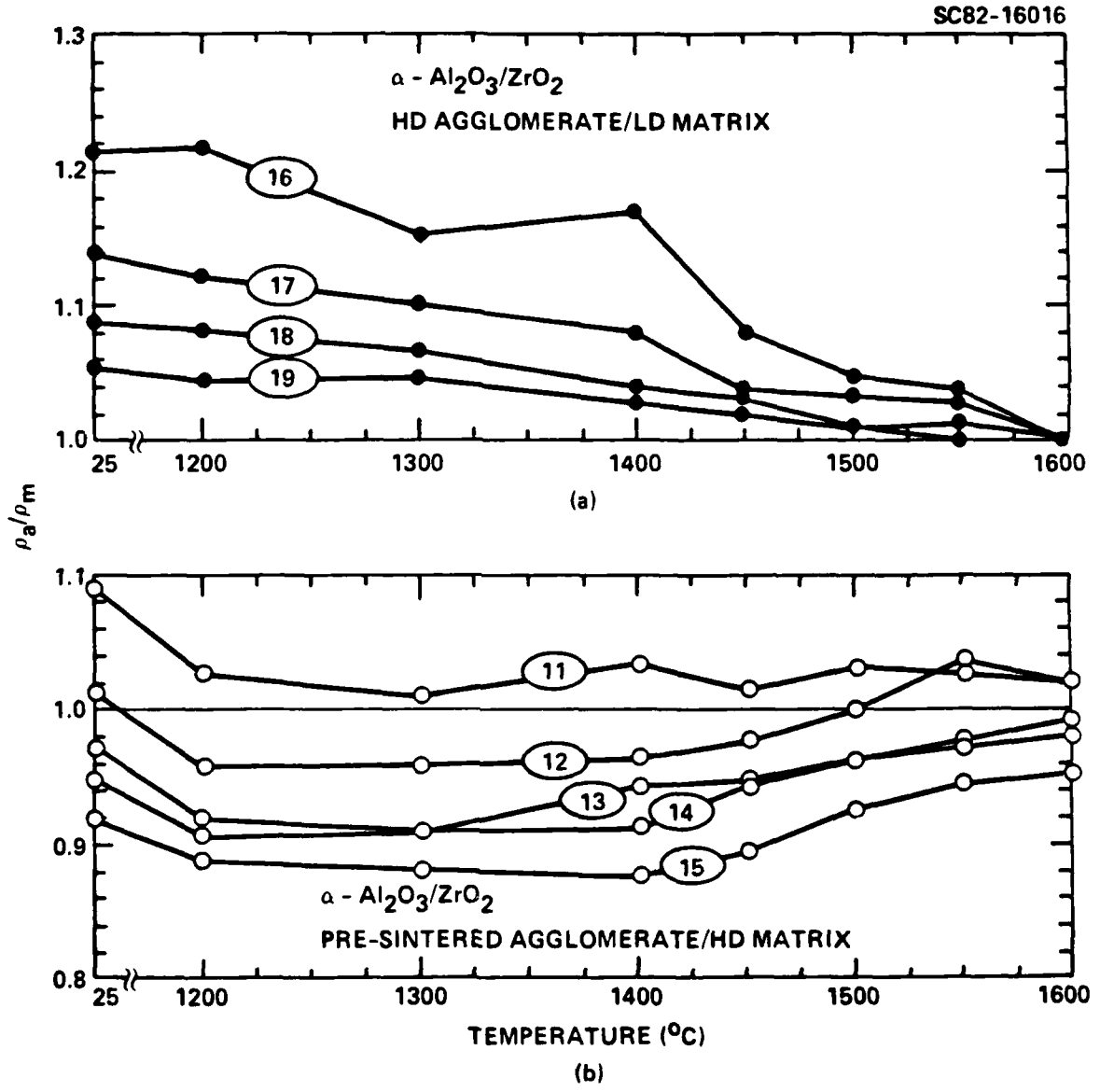

Fig. 7 Density ratio of the agglomerate (ρ_a) and its respective matrix (ρ_m) as a function of cyclic sintering temperature for specimens fabricated with the α-Al_2O_3/ZrO_2 composite powder.

transformations in the matrix surrounding the pre-sintered agglomerates which had already undergone these shrinkage phenomena. Compressive strains were exerted on the agglomerate during this portion of the sintering cycle. For some of the specimens (12-15, see Fig. 7), ρ_a/ρ_m became $>\rho_{oa}/\rho_{om}$ in a latter portion of the sintering schedule. During this latter portion, the differential strain was tensile (see Eq. (3)).

5.3 Perturbations in the Matrix Strain Field Due to Differential Sintering

Figure 8 illustrates the perturbations in the original orthogonal grid pattern produced by differential sintering for the case where ρ_a/ρ_m was persistently less than ρ_{oa}/ρ_{om} during the full sintering schedule.* The radial and tangential strains in the matrix were determined as a function of (r/R) for a pattern similar to that shown in Fig. 8; R is the agglomerate radius and r is the radius vector. As shown in Fig. 9, the radial and tangential strains within the matrix can be represented as

$$\varepsilon_v = \varepsilon_m + 2\Delta\varepsilon \left(\frac{R}{r}\right)^3$$

and

$$\varepsilon_t = \varepsilon_m - \Delta\varepsilon \left(\frac{R}{r}\right)^3 \quad ,$$

where ε_m is the matrix strain at $R/r \to 0$ and $\Delta\varepsilon = \varepsilon_m - \varepsilon_a$. In the plot illustrated by Fig. 9, $\varepsilon_a = 0$ (specimen 1, 1200°C). Thus, for the cases where $\rho_a/\rho_m < \rho_{oa}/\rho_{om}$, the lower densification rate of the agglomerate restricts the tangential shrinkage strain by $\Delta\varepsilon(R/r)^3$ and enhances the radial shrinkage by $2\,\Delta\varepsilon(R/r)^3$.

*Note the many raised areas on the matrix surface (see arrows). These are agglomerates in the powder which were uplifted due to differential sintering. They are ~ 0.1 the size of the agglomerate which was artificially introduced.

SC82-15944

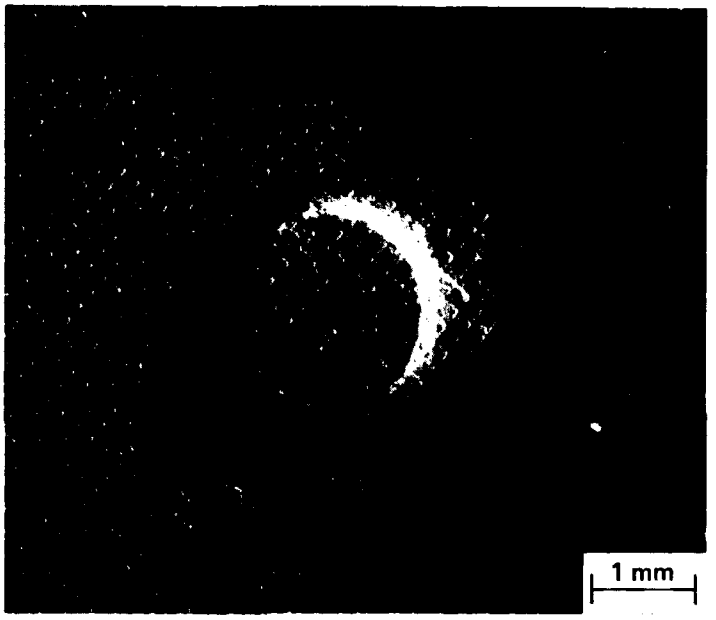

Fig. 8 Perturbations produced in the original orthogonal grid pattern by differential sintering; case where $\rho_a/\rho_m < \rho_{oa}/\rho_{om}$. (Specimen 1, 1600°C). Arrow indicates the size of agglomerates in the powder which were raised above the surface due to differential sintering.

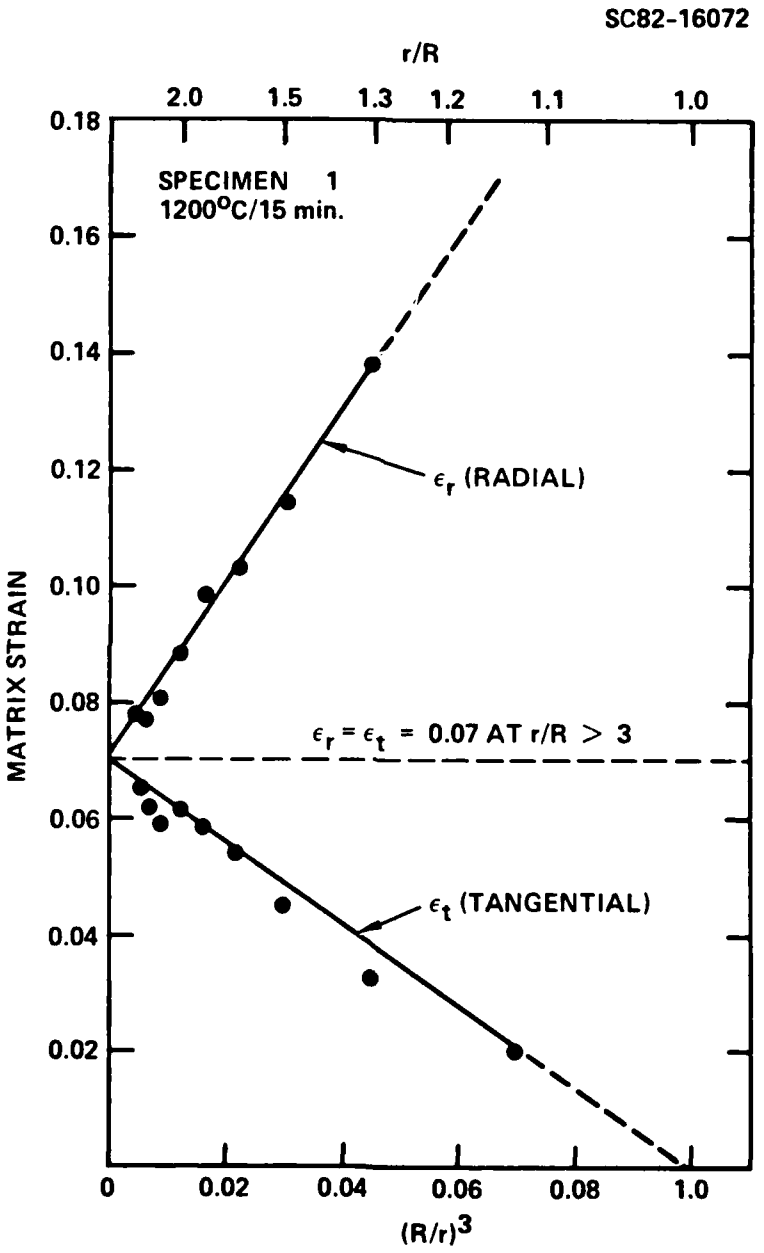

Fig. 9 Radial (ϵ_r) and tangential (ϵ_t) strains in matrix as a function of $(R/r)^3$. R = radius of agglomerate, r = radius vector. Case where $\rho_a/\rho_m < \rho_{oa}/\rho_{om}$.

For the cases where the agglomerate persistently densified at a faster rate relative to the matrix (specimens containing lower density agglomerates fabricated by Route II in Fig. 2), the agglomerate separated from the matrix and did not perturb the orthogonal grid pattern in the adjacent matrix. However, for those specimens fabricated through Route I containing pre-sintered, lower density agglomerates, where initially $\rho_a/\rho_m < \rho_{oa}/\rho_{om}$ but finished with $\rho_a/\rho_m > \rho_{oa}/\rho_{om}$ (specimens 12-15, Fig. 7), the strain pattern in the adjacent matrix reversed itself from the pattern where ε_t and ε_r were restricted and enhanced respectively (similar to that shown in Fig. 8), to the pattern where ε_t was enhanced and ε_r was restricted. This reversal was observed in the latter stage of the sintering schedule when $\rho_a/\rho_m > \rho_{oa}/\rho_{om}$. Although this reversed pattern was certainly perceptable by sighting along the grid lines adjacent to the agglomerate, the magnitude of the strain was insufficient to obtain accurate values of ε_r and ε_t as a function of the radial vector with the size of the orthogonal grid used in these experiments.

5.4 Surface Profile

Profilometer traces were very instructive in relating the interaction of the agglomerate with the matrix due to differential sintering. Figure 10 illustrates the profiles* after each successive sintering temperature for two examples where ρ_a/ρ_m was persistently $< \rho_{oa}/\rho_{om}$ throughout the sintering schedules (specimens 6-10 and 16-19, Figs. 6 and 7). These two examples represent the cases where ρ_{oa}/ρ_{om} was large (Fig. 10a, $\rho_{oa}/\rho_{om} = 1.21$)and small (Fig. 10b, $\rho_{oa}/\rho_{om} = 1.02$). The broken line on these profiles represents the agglomerate's perimeter, as determined by measurements made on calibrated micrographs after each sintering cycle.

The interaction depicted in Fig. 10 will be detailed first with respect to the agglomerate, then with respect to the matrix. As differential sintering

*The orthogonal grid pattern was omitted when the originals were traced for the figures. Note the differences in horizontal and vertical scales.

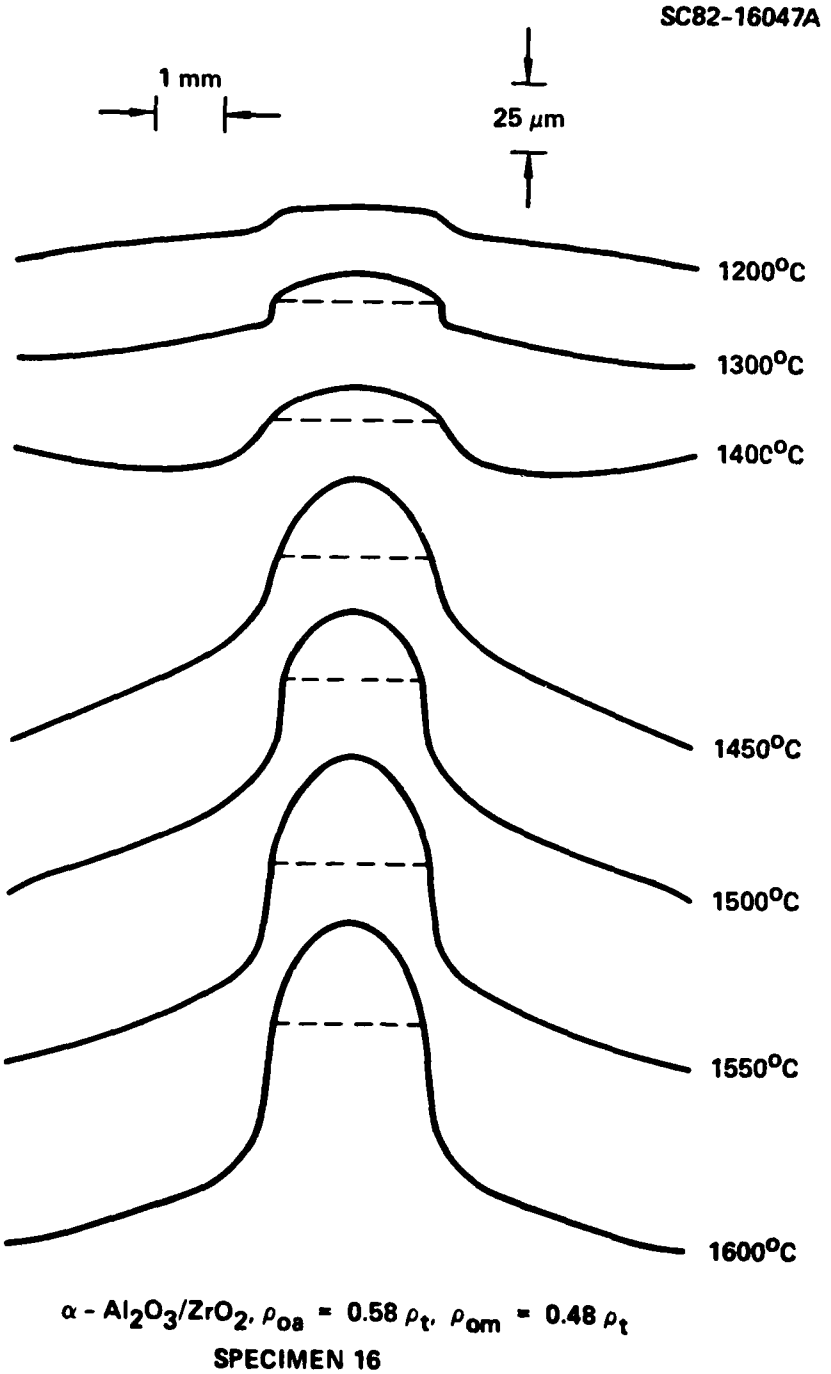

Fig. 10 Surface profiles after each sintering cycle for two cases where $\rho_a/\rho_m < \rho_{oa}/\rho_{om}$.

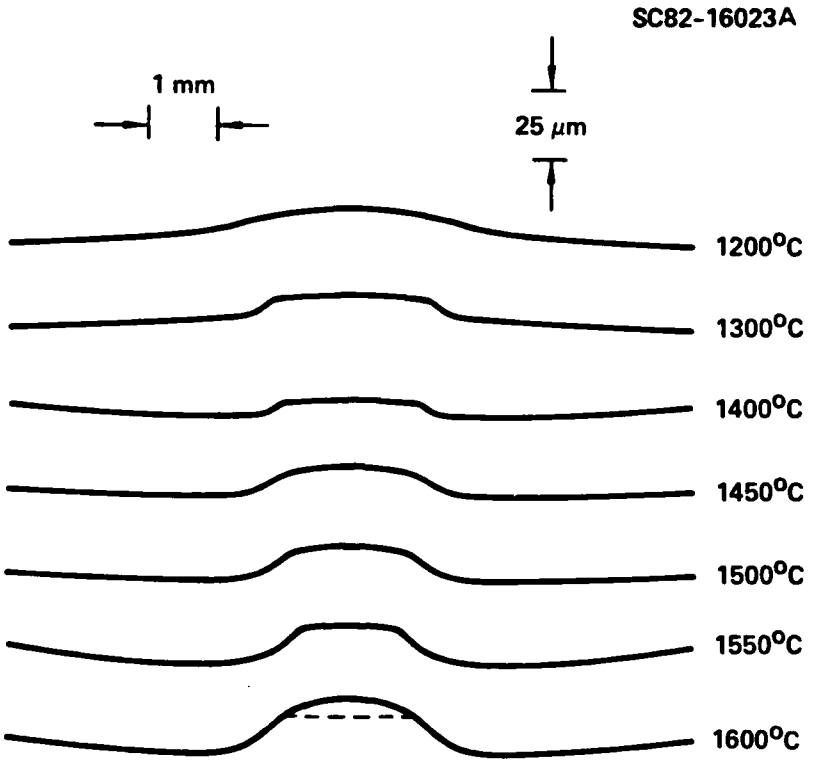

γ - Al_2O_3/ZrO_2, ρ_{oa} = 0.48, ρ_{om} = 0.47
SPECIMEN 10

Fig. 10b

proceeds, the agglomerate protrudes above the specimen's surface. The extent of the protrusion was proportional to both ρ_{oa}/ρ_{om} and temperature. As the protrusion proceeds, the initial flat surface of the agglomerate develops a crown. The height of the crown was proportional to ρ_{oa}/ρ_{om} and temperature. The total height (X) of the protrusion above the matrix surface (at r/R = 2) and the height of the protrusion to the agglomerate's perimeter (Y) (i.e., excluding the crown height) were determined as a function of $\Delta\varepsilon$ (ε_m and ε_a were determined from displacements of the orthogonal surface grid) are shown in Figs. 11 and 12 for specimens fabricated with the two different composite powders. Figures 11a and 12a show the height of the protrusion excluding the crown height (Y) as a function of $\Delta\varepsilon$. The solid lines in Figs. 11a and 12a were determined by using the initial radii (R_o) of the hemispherical agglomerates to calculate the expected protrusion as a function of $\Delta\varepsilon$ if the agglomerates were neither bonded nor constrained by the matrix, viz $Y = R_o\ (\varepsilon_m - \varepsilon_a)$. The shaded area is bounded by the maximum and minimum radii of the agglomerates. As shown, the height of the protrusion excluding the crown is nearly coincident (within experimental error) with the expected height. Figures 11b and 12b show that when the crown is included in the protrusion height, the agglomerate's protrusion height can be up to twice the expected height. The extent of the extra protrusion is approximately equal to the crown height.

Figure 10 illustrates that the displacement of the matrix surface due to the interactive, differential sintering for the case where $\rho_a/\rho_m < \rho_{oa}/\rho_{om}$ can extend to large radial distances ($r/R > 5$), particularly when $\rho_{oa}/\rho_{om} > 1.10$. The displacement of the matrix surface can be characterized by two phenomena. First, with only few exceptions, the agglomerate/matrix interface appears well enough bonded that the shape of the surface between $0 > r/R > 2$ can be described by a smooth, step-free curve which has a single inflection; the inflection point is coincident with the agglomerate/matrix interface. One of the exceptions is shown in Fig. 10a at 1300°C, where a step exists at the agglomerate/matrix interface. The other exceptions also occurred at the low temperature range of the sintering schedule, where agglomerate/matrix bonding was apparently the weakest.

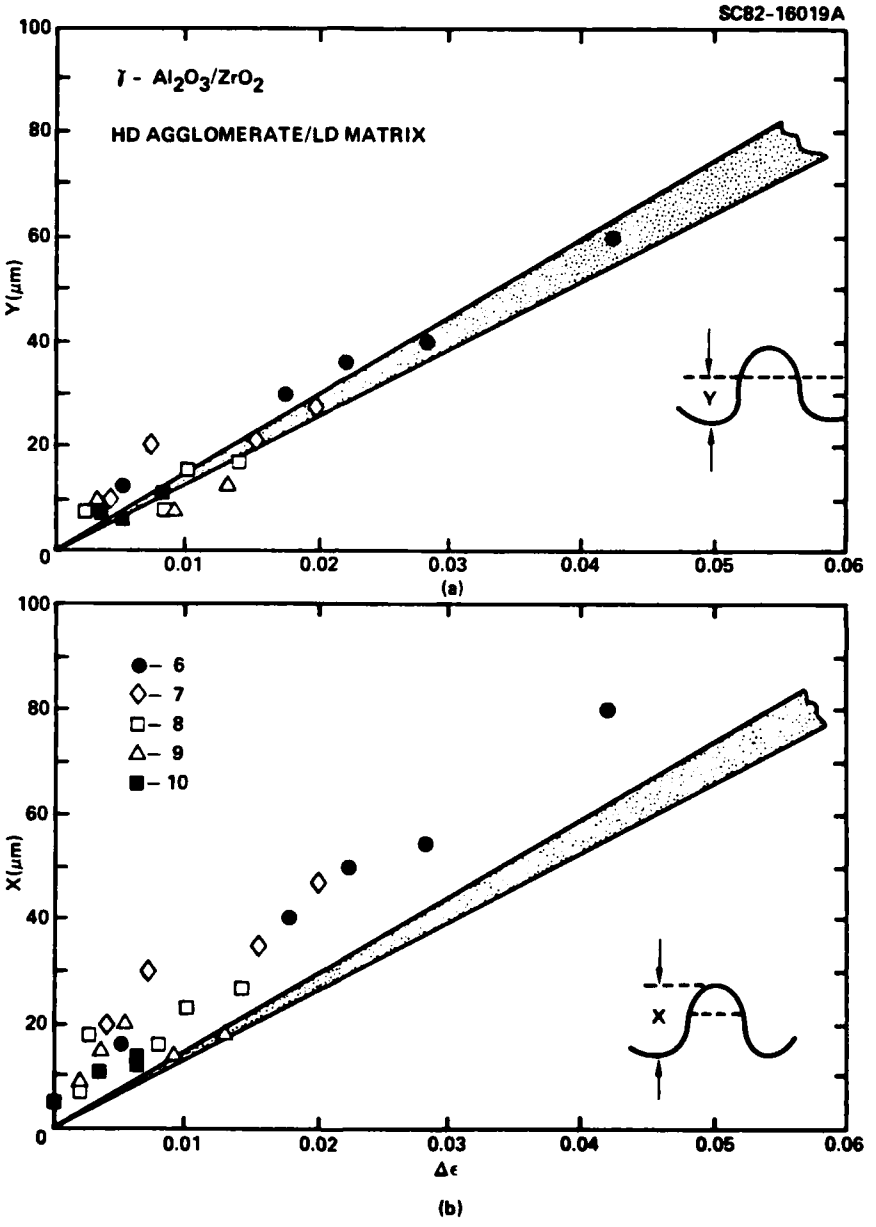

Fig. 11 Protrusion heights vs differential strain ($\Delta\varepsilon = \varepsilon_m - \varepsilon_a$) for high density agglomerates within lower density matrices. a) Y = height excluding crown height, b) X = total protrusion height. Specimens fabricated with γ-Al_2O_3/ZrO_2 composite powders.

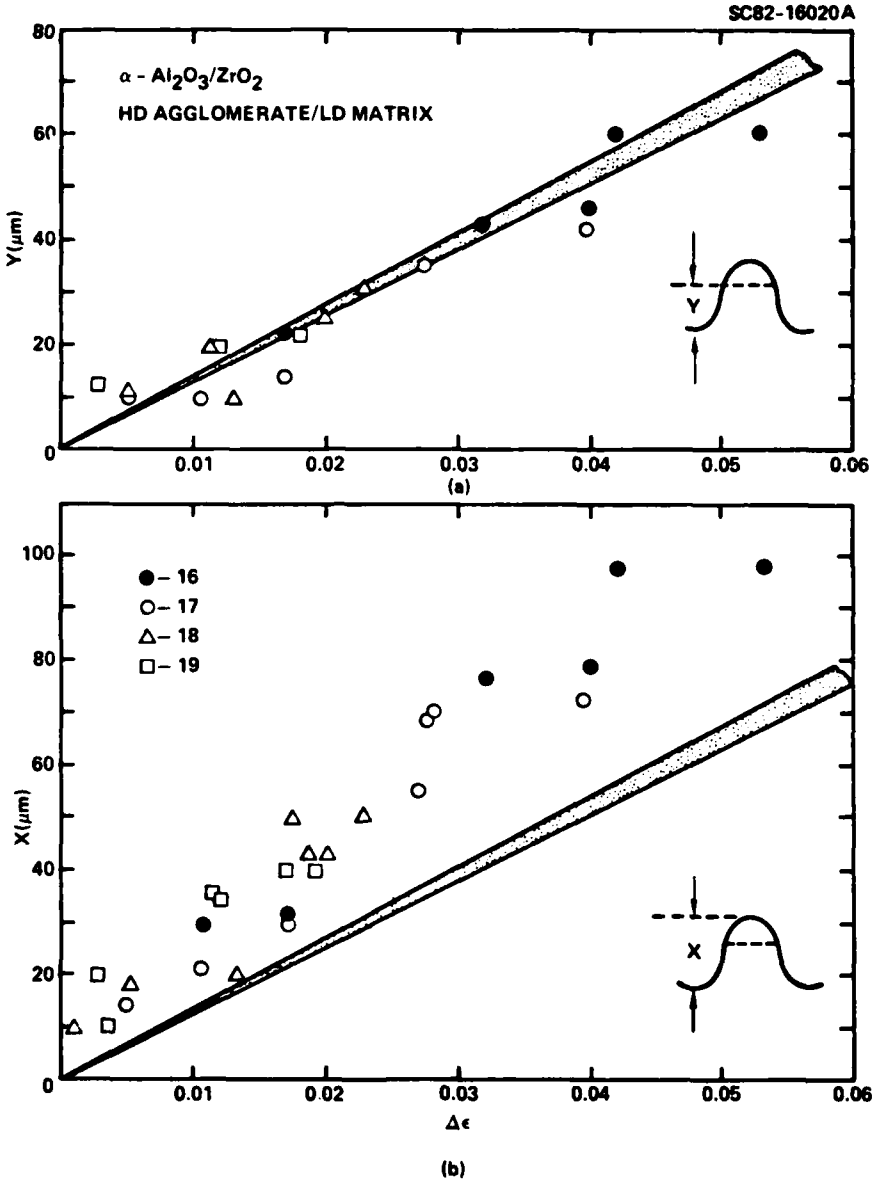

Fig. 12 Protrusion heights vs differential strain ($\Delta\varepsilon = \varepsilon_m - \varepsilon_a$) for high density agglomerates within lower density matrices. a) Y = height excluding crown height, b) X = total protrusion height. Specimens fabricated with α-Al_2O_3/ZrO_2 composite powders.

The second phenomenon is the deviation of the initially planar matrix surface. As shown in Fig. 10, the matrix surface ($r/R > 1$) can either be up-lifted or depressed relative to the initial planar surface. In all cases, the up-lifting (defined as a displacement in the direction of the outward normal to the initial planar surface for all r/R) occurred first (e.g., see Fig. 10, 1200°C and 1300°C). As differential sintering proceeded at higher temperature, the up-lifted surface became depressed, as shown in Fig. 10a at 1400°C and Fig. 10b for $1 \geq r/R \geq 2$. As differential sintering proceeded even further, the depressed surface could again become up-lifted, as shown in Fig. 10a, $T \geq$ 1450°C, or remain depressed as shown in Fig. 10b. In all cases, as end-point densities were approached at the highest temperature (1600°C), all matrix surfaces tended to become planar as they started. This outward (up-lifting) and inward (depressing) displacement of the matrix surface will be related to other information in a latter section.

Figure 13 illustrates the sequential surface profiles for specimens fabricated with pre-sintered agglomerates. Figure 13a is representative of the case where ρ_a/ρ_m was persistently $< \rho_{oa}/\rho_{om}$ throughout the sintering schedule; Fig. 13b is representative of the case where ρ_a/ρ_m decreased during the initial portion of the schedule and then increased to become $> \rho_{oa}/\rho_{om}$ during the last portion of the schedule. The major differences with respect to the cases discussed above (Fig. 10) are as follows. First, the largest protrusion of the agglomerate occurred during the initial heating, coincident with the large decrease in ρ_a/ρ_m (Figs. 6 and 7) and coincident with the differential shrinkage due to the $\gamma \rightarrow \alpha$ - Al_2O_3 and $m \rightarrow t$ - ZrO_2 transformations of the matrix relative to the pre-sintered agglomerate. Second, the height of the protrusion decreased as sintering proceeded; this is again coincident with the increase of ρ_a/ρ_m from its minimum value. Third, as shown in Fig. 13b, the agglomerate became depressed below the matrix surface when $\rho_a/\rho_m > \rho_{oa}/\rho_{om}$.

A sequential set of profiles could not be obtained from specimens containing the low density agglomerates fabricated by Route II (see Fig. 2). For these specimens, the lower density agglomerate partially separated from the

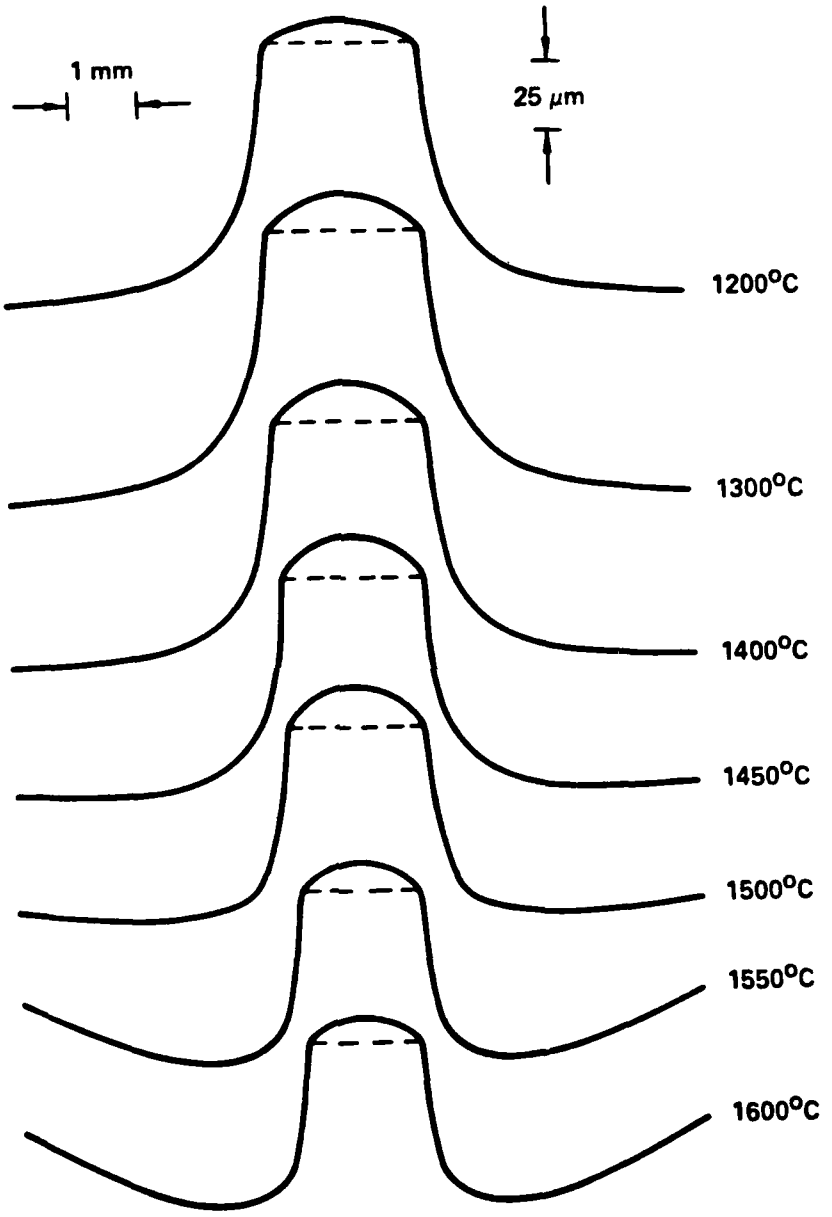

Fig. 13 Surface profiles after each sintering cycle for two specimens containing presintered agglomerates.

SC82-16045

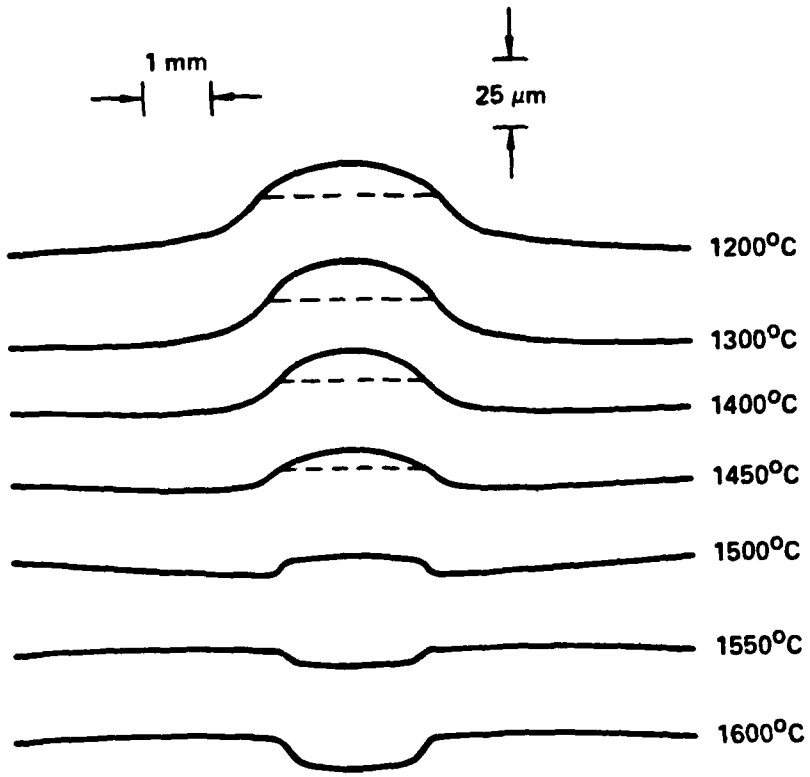

α - Al_2O_3/ZrO_2, ρ_{oa} = 0.52 ρ_t, ρ_{om} = 0.57 ρ_t

SPECIMEN 15

Fig. 13b

higher density matrix during the initial portion (1200°C to 1400°C) of the sintering schedule. The stylus on the profilometer would break the remaining bonded portion and cause the agglomerate to rotate, thus ruining the specimen for further experimentation. Figure 14 illustrates the extent to which the agglomerate separates from the matrix (dashed line) for a specimen heated to 1600°C/1 hr without observations at intermittent temperatures. The highlighting produced by the oblique lighting also shows that the agglomerate is tilted, i.e., protruding above the matrix surface in the bonded region and depressed below the surface in the unbonded region.

5.5 Cracks Produced by Differential Sintering

Figure 14 illustrates the typical circumferential crack developed at the agglomerate/matrix interface for all cases examined (ρ_{oa}/ρ_{om} F 0.97) where the green density of the agglomerate was less than that of the matrix and the agglomerate was not pre-sintered. The maximum separation distance was not measured, but it appeared to be proportional to the differential green density. The same results were obtained when an agglomerate formed from γ-Al_2O_3/ZrO_2 was incorporated into a matrix of α-Al_2O_3/ZrO_2. Here, the $\gamma \rightarrow \alpha$-$Al_2O_3$ transformation, the lower green density of the γ-Al_2O_3/ZrO_2 agglomerate (compacted at the same isostatic pressure), and the smaller particle size of the γ-Al_2O_3 all contributed to the faster densification rate for the agglomerate relative to the matrix.

Of the specimens containing the pre-sintered agglomerates, only 11 and 12 contained crack-like separations due to differential sintering. The example in Fig. 15 shows the sectioned specimen (sectioned surface - gray; top surface - dark), illustrating that the separation circumvents all but the bottom portion of the agglomerate/matrix interface. For both specimens, $\rho_{oa}/\rho_{om} > 1$ and the value of ρ_a/ρ_m at the end of the sintering schedule was $> \rho_{oa}/\rho_{om}$ for specimen 12 (see Fig. 7); sequential profiles were similar to that shown in Fig. 13a.

SC82-15945A

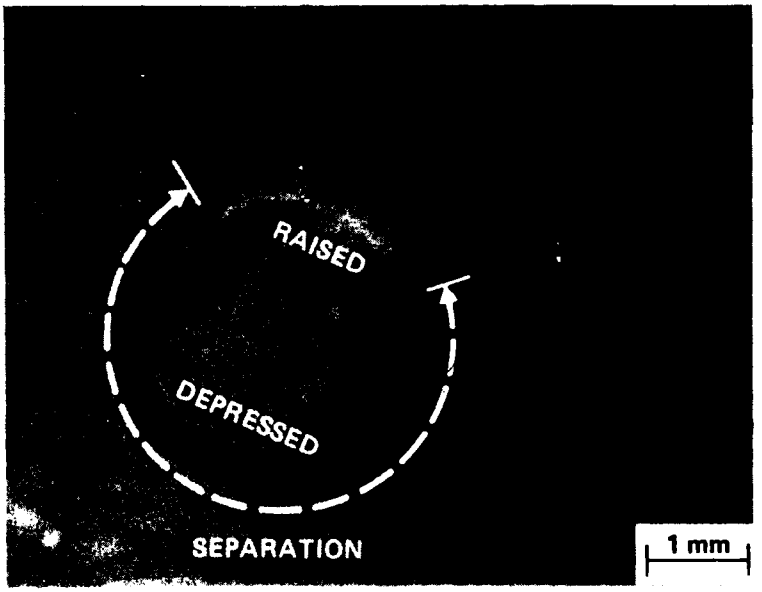

Fig. 14 Photograph of low density agglomerate which separated from its higher density matrix due to differential sintering. Extent of circumferential separation is indicated by the broken line.

SC82-16813

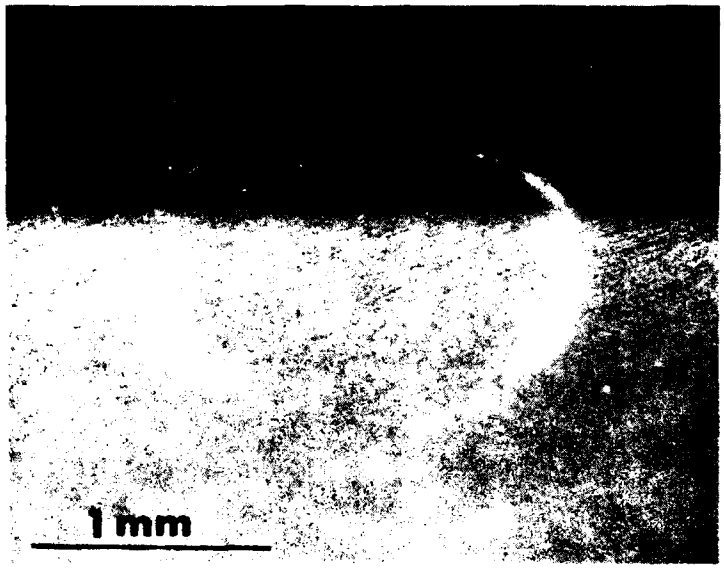

Fig. 15 Photograph of specimen 12 which was sectioned and penetrated to reveal the crack shown as a white, diffuse line that extends around the agglomerate/matrix interface except at the bottom of the agglomerate. Dark surface is the specimen's exterior and grey surface is the sectioned surface.

Four types of crack-like separations were observed in specimens containing the higher density agglomerates ($\rho_{oa}/\rho_{om} > 1$). Specimen 16 ($\rho_{oa}/\rho_{om} = 1.21$) contained circumferential agglomerate/matrix separation similar to that shown in Fig. 14. In addition, it also contained lateral cracks that circumscribed the bottom of the agglomerate, as shown in Fig. 16 which also shows the partially sintered separation that circumvents most of the agglomerate/matrix interface.

As shown in Fig. 17, radial crack-like separations were observed in specimens 9 and 10 (bleeding of the phosphorescent dye greatly exaggerates the separation width). Specimen 9 only contained one radial separation relative to specimen 10 shown in Fig. 17.

The fourth and last was a crack-like separation that traversed the top portion of the agglomerate, as shown in Fig. 18. This only occurred in specimen 6. Observations at higher magnification indicated that this transverse separation was partially sintered closed. Although the matrix of specimen 6 was somewhat porous (88% of theoretical density) and absorbed dye-penetrant, observations at higher magnification indicated the presence of circumferential and lateral cracks which were similar to, but not as well defined as those shown in Fig. 16.

No cracks were observed in the other specimens.

Since the principal observations for the crack-like separations were made by dye penetrating the specimens after the last stage of the sintering cycle, it was difficult to determine, without ambiguity, the point within the sintering schedule at which the crack first initiated. Studies of the photographs taken after each sintering cycle indicated that the radial cracks associated with specimens 9 and 10 initiated during the 1450°C cycle, where they appeared as fine lines. Further sintering caused the cracked surfaces to slightly separate, but they went unnoticed until the dye penetrant was employed.

Three observations suggest that the circumferential cracks initiated during the cycle where the matrix adjacent to the agglomerate became depressed (e.g., Fig. 10a, 1400°C). First, a separation was observed at the agglomerate/matrix interface for specimens which underwent large depressions during one

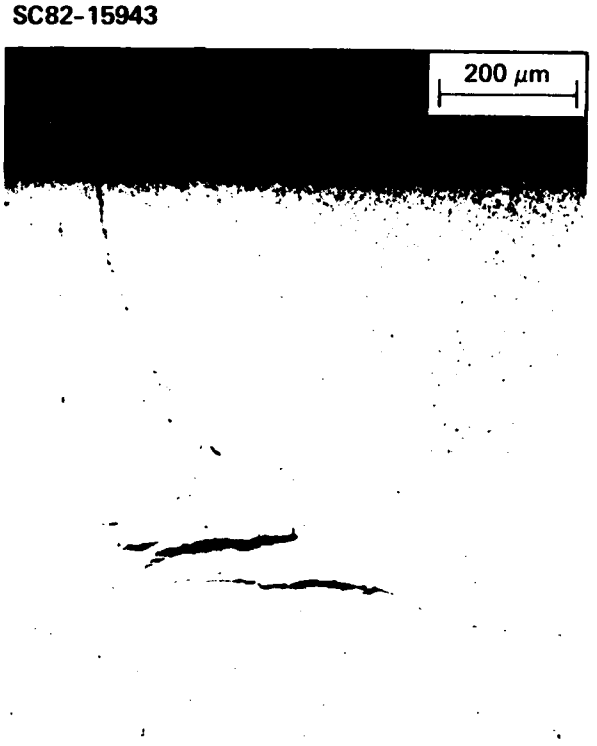

Fig. 16 Sectioned view of specimen 16 showing lateral cracks that circumscribe the bottom of the agglomerate. A high magnification of the agglomerate/matrix separation showed that the crack located at this interface was partially sintered together.

SC82-15947A

Fig. 17 Radial crack-like separations developed in specimen 10 due to differential sintering.

SC82-15946A

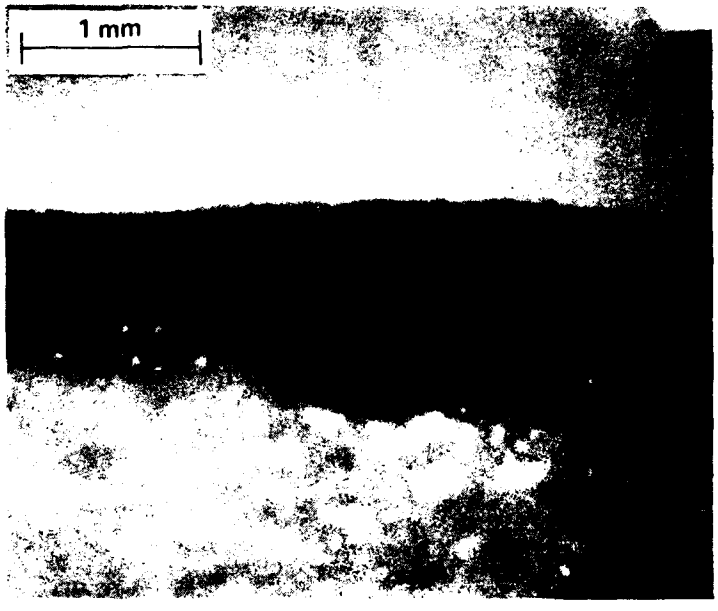

Fig. 18 Partially sintered crack that traverses the top of the agglomerate in specimen 6 shown in a section view. Also note the denser surface relative to the less dense version (interior absorbs the dye-penetrant).

cycle. Second, the separation between the surfaces of the circumferential crack appeared to decrease when the matrix underwent its second up-lifting. Third, after the end of the sintering schedule, the cracked surfaces were partially sintered together, suggesting that the cracked surfaces were compressed upon the second up-lifting.

Although no direct evidence exists, it can be argued that the stress system existing during the up-lifting of the matrix is consistent with the formation of the lateral cracks. For example, lateral cracks associated with surface indentation occur when the indentor is unloaded and removed from the surface.[13] That is, it is not inconsistent to suggest that the lateral cracks form during the second up-lifting of the matrix.

The transverse crack within the agglomerate was partially healed, suggesting that it initiated during an intermediate cycle by tensile stresses due to the development of the crown surface on the agglomerate. Since the only transverse crack observed coincided with one of the orthogonal grid lines, it was not observed prior to dye penetration.

6. Discussion

Within the range of experimental variables investigated, it was shown that densification rates are inversely proportional to green density. This conclusion agrees with Bruch's early observations for what he defined as the normal sintering regime. Phenomena associated with Bruch's sub-normal sintering regime, viz. densification rate proportional to green density, were not observed within the present experimental framework.

Neglecting for the moment the phenomena produced by pre-sintered agglomerates, it was clearly shown that when the green density of the agglomerate was less than the matrix, the agglomerate would densify at a greater rate to form large, crack-like internal voids bounded by most of the agglomerate/ matrix interface. From the standpoint of densification, it can be quickly perceived that if a powder compact contains many lower density agglomerates, end-point densities will be less than theoretical due to the crack-like voids. A geometric analysis of this problem relating the fraction porosity (P) produced by

differential sintering to the volume fraction (V_a) of low density agglomerates results in

$$P = \frac{\rho_{om} - \rho_{oa}}{\rho_t} V_a \quad .$$

With this simple model, conditions can easily be perceived where $0.01 > P > 0.10$. Theoretical density could be achieved in these situations if the crack-like voids were "relocated" to positions that are thermodynamically more favorable to their disappearance by volume diffusion. This could be accomplished by grain growth, viz. a development of a new microstructure where the grain size exceeds the agglomerate sizes and thus exceeds the size of the void initially produced by the agglomerate. In light of the above discussions, the effect of an applied pressure during sintering (viz. hot-pressing) now takes on a new and, possibly, domineering role. That is, the applied pressure prevents the formation of crack-like voids due to differential sintering which allows the achievement of theoretical density at smaller grain sizes. A similar idea was put forth by Morgan[12] for hot-pressing conditions involving decomposition reactions.

From the viewpoint of strength, the crack-like void produced by the differential sintering of the low density agglomerate is a potential fracture origin. Since the size of the crack-like void is proportional to the agglomerate size, and strength is inversely proportional to the square-root of the crack size, one would expect that the strength would be inversely proportional to the square-root of the agglomerate size. Also, the distribution of strength values will mimic the size distribution of the agglomerates. Namely, strength can be increased by decreasing the agglomerate size, and a narrow strength distribution should be achieved with a narrow size distribution of agglomerates.

It was also clearly shown that when the green density of the matrix was less than the agglomerate, the matrix would densify more rapidly and exert a compressional strain on the agglomerate. The agglomerate, resisting the compressional strain exerted by the matrix, alters the strain field in the adjacent matrix, as shown in Fig. 9. It is obvious that the resistance of the ag-

glomerate to the strain exerted by the matrix sets up a stress field within and around the agglomerate.

It has been shown that this stress field had various effects. First, and somewhat unanticipated, it can cause agglomerates to be mobile. For the majority of the cases examined, the agglomerate was located on the surface and, by definition, the stress field is non-symmetric with respect to the surface normal. The net force produced by this non-symmetric stress field acts on the agglomerate to push it through the surface, somewhat analogous to squeezing a slippery bar of soap. This net force is evident by the significantly larger protrusion of the agglomerate than expected (see Figs. 11 and 12). If the agglomerate were completely submerged within a matrix of uniform density distribution, the expected stress field would be symmetric, the net force acting on the agglomerate would be zero, and thus the agglomerate would be immobile. This situation might be expected to be highly improbable. That is, the matrix's density distribution around the agglomerate may not be completely uniform, producing a net force and hence mobility of the submerged agglomerate.

Mass rearrangement by agglomerate mobility takes place over much greater distances that can ever be expected through diffusional processes. More open, lower green density matrices would be expected to offer less resistance to agglomerate mobility. If the mass rearrangement produced by agglomerate mobility would lead to a more sinterable microstructure, it would explain why lower green density compacts initially exhibit greater densification rates.

Second, the constrained upward movement of the surface agglomerate produces a crown on the agglomerate. This shape suggests that although the lower portion of the agglomerate may be in a state of compression, its surface is in a state of tension, as evident by the crack that traverses the upper portion of the agglomerate shown in Fig. 18.

Third, the uplifting of the agglomerate also produces an uplifting of the adjacent matrix. When this uplifting is significant, the matrix breaks away from the agglomerate to form a circumferential, crack-like separation (see Figs. 15 and 16), which allows the surrounding matrix to densify to produce a depressed matrix surface (Fig. 10) surrounding the agglomerate. With further

differential sintering, the matrix again exerts compressional stresses on the agglomerate which attempts to close the circumferential crack-like separation, producing a second uplifting of the matrix adjacent to the agglomerate and the formation of lateral cracks as shown in Fig. 16.

Fourth, when the uplifting is insignificant (Fig. 10b), the tangential tensile stresses generated in the matrix adjacent to the agglomerate produce radial cracks, as shown in Fig. 17.

Thus, the stress distribution produced by the greater sintering rate of a matrix relative to the agglomerate not only results in agglomerate mobility and microstructure rearrangement, but also can result in a variety of crack-like internal surfaces which will decrease the potential strength of the sintered body, as discussed above.

It was also shown that phase transformations (e.g., $\gamma \rightarrow \alpha\text{-}Al_2O_3$ and $m \rightarrow t\text{-}ZrO_2$) also produce differential strains. For the cases studied, the transformations and the accompanying differential strains occurred prior to the temperature range where diffusional processes resulted in substantial sintering. That is, agglomerate mobility and microstructure rearrangement due to phase transformations occurred at the lower temperature range before real sintering had started.

In conclusion, the results presented above only reinforce current thinking that agglomerates must be eliminated from powder processing. They point out that agglomerates are not only detrimental from the standpoint of sintering behavior, but also detrimental in the attempts to achieve a reliable, structural material. It is obvious that scientific and technical priorities must be placed on powder routes that avoid hard agglomerates and powder processing routes that prevent soft agglomerates from developing during consolidation.

Acknowledgements

This work was performed under contract to the Air Force Office of Scientific Research, Contract No. F49620-81-0036.

References

1. F.F. Lange, "Processing Related Fracture Origins: Part 1, Observations in Sintered and HIP-Treated Al_2O_3/ZrO_2 Compositions," (to be published).

2. I.A. Aksay, B.I. Davis and F.F. Lange, "Dispersion Stability of Al_2O_3/ZrO_2 Colloidal Suspensions," (to be published).

3. J. Selsing, "Internal Stresses in Ceramics," J. Am. Ceram. Soc. 44, 419 (1961).

4. J.D. Eshelby, "Elastic Inclusions and Inhomogeneities," Progress in Solid Mechanics, Vol. 2 Ed. by In.N. Sneddon and R. Hill, p. 89 North-Holland (1961).

5. R.W. Davidge and T.J. Green, "The Strength of Two-Phase Ceramic/Glass Materials," J. Mat. Sci. 3, 629 (1968).

6. D.R. Green, "Microcracking Mechanisms in Ceramics," Fracture Mechanics of Ceramics, Ed. by R.C. Bradt, A.G. Evans, D.P.H. Hasselman and F.F. Lange (in press with Plenum).

7. F.F. Lange, "Criteria for Crack Extension and Arrest in Residual, Localized Stress Fields Associated with Second Phase Particles," Fracture Mech. of Ceram. Vol. 2, Ed. by R.C. Bradt, D.P.H. Hasselman and F.F. Lange, p. 599, Plenum (1974).

8. C.A. Bruch, "Sintering Kinetics for the High Density Alumina Process," Bul. Am. Ceram. Soc. 41, 799 (1962).

9. C. Greskovich, "Effect of Green Density on the Initial Sintering of Alumina," Physics of Sintering, 4 33-46 (1972).

10. T. Vasilos and W. Rhodes, "Fine Particulates to Ultrafine-Grain Ceramics," Ultrafine-Grain Ceramics, Ed. by J.J. Burke, N.L. Reed and V. Weiss, pp. 137-72, Syracuse University Press (1970).

11. F.F. Lange, B.I. Davis and D.R. Clarke, "Compressive Creep of Si_3N_4/MgO Alloys: Part 1, Effect of Composition," J. Mat. Sci. 15, 601 (1980).

12. P.E.D. Morgan and E. Scala, "Formation of Fully Dense Oxides by Pressure Calcintering of Hydroxides," Proc. 2nd Int. Conf. on Sintering and Related Phenomena," Ed by G.CV. Kuczynski, N.A. Hooton and C.F. Gibbon, Gordon and Breach, pp. 861-94 (1967).

13. B.R. Lawn and D.B. Marshall, "Indentation Fracture and Strength Degradation in Ceramics," (ibid Ref. 7), Vol. 3, pp. 205-30 (1978).

APPENDIX III
PROCESSING RELATED FRACTURE ORIGINS: PART 3, DIFFERENTIAL SINTERING OF ZrO_2 AGGLOMERATES IN Al_2O_3/ZrO_2 COMPOSITE

F.F. Lange, I.A. Aksay* and B.I. Davis

Abstract

Large ZrO_2 hard agglomerates remained in an Al_2O_3/ZrO_2 composite suspension after inefficient ball milling. The ZrO_2 agglomerates shrank away from the consolidated Al_2O_3/ZrO_2 powder matrix during sintering, producing crack-like voids which were responsible for strength degradation.

Introduction

It was previously demonstrated that dry powder routes to powder consolidation can produce large agglomerates which result in large crack-like voids due to differential sintering.[1] In the dry powder routes, the agglomerates are apparently formed either by the spontaneous attraction of particles due to Van der Waals forces or by particle cohesion due to surface tension effects produced by absorbed, atmospheric water. It was also demonstrated that the colloidal/filtration route (commonly known as slip casting) to powder consolidation has great potential for minimizing agglomerate size and therefore the size of the strength degrading crack-like voids formed by differential sintering.[2] The objective of this route is to break down all agglomerates and to keep the particles well dispersed in a liquid, using the principles of either electrostatic repulsion or steric hinderance, up to the last moment when most of the liquid is removed by filtration. This communication will point out that theory is sometimes difficult to achieve in practice and will catalog another type of agglomerate which produces strength-degrading crack-like voids and how it is related to powder processing.

*Department of Materials Science and Engineering, University of California, Los Angeles.

Experimental

The initial intention of this work was to reproduce the procedure to make a high strength Al_2O_3/ZrO_2 material by the colloidal/filtration route described earlier,[2] but to avoid the silicate phase that produce the strength limiting flaws observed at the fracture origins. In the original work,[2] the silicate phase was traced to the debase-Al_2O_3 mill jar and milling media. Thus, the only known change made was to use a high-purity Al_2O_3 mill jar and milling media purchased* for this task. As reported earlier,[2] the ZrO_2 powder† comprises sub-micron particles. Many of these particles form larger, hard agglomerates which can only be broken down by attrition. The Al_2O_3§ powder is relatively free of hard agglomerates. As before, the two powders (Al_2O_3/30 v/o ZrO_2) were combined with deionized water at pH 2.5 to produce a suspension containing 25 v/o solids, milled for 18 hrs, readjusted to pH 2.5, filtered, dried, sintered at 1600°C/2 hrs, and cut into specimens for flexural strength determinations (inner span: 1.27 cm; outer span: 2.54 cm).

Results and Discussion

Strength values were significantly lower than those previously reported, with values ranging between 510 MPa and 572 MPa and an average of 540 MPa.

Fracture origins were examined in a SEM to determine if the strength degrading flaws could easily be traced to some processing step. In all cases, a large polycrystalline ZrO_2 inclusion contained within a similarly shaped, but somewhat larger hole was observed at the fracture origin, as shown by the typical example in Fig. 1a. A matting hole was observed at the fracture origin on the other half of the fractured specimen. At higher magnifications it could be seen that the topography of the surfaces within the hole and those bounding the ZrO_2 inclusion were internal, sintered surfaces as distinct from the

*Coors Porcelain Co., Golden, CO: 99.5% Alumina grinding media.
†Zircar Products, Florida, NY.
§ALCOA, Pittsburgh, PA; >99.5% α-Al_2O_3.

SC82-16786

Fig. 1a ZrO_2 polycrystalline inclusion at fracture origin.

SC82-16787

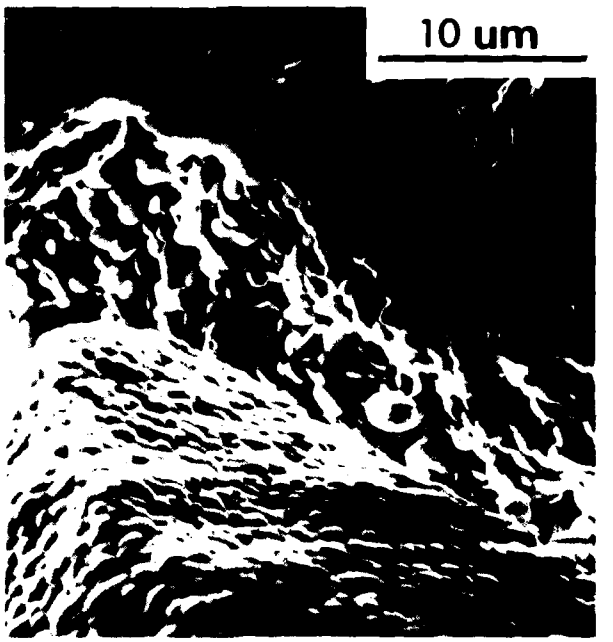

Fig. 1b Micrograph showing that ZrO_2 inclusion surface and Al_2O_3/ZrO_2 surface from which the ZrO_2 agglomerate had separated are internal, sintered surfaces.

topography of the surrounding fracture surfaces as shown in Fig. 1b. Smaller ZrO_2 inclusions which were separated from the composite Al_2O_3/ZrO_2 matrix with a crack-shaped void were also observed on the fracture surfaces but remote from the fracture origin, as shown in Fig. 2a. Such crack-like voids were too small to be the strength degrading flaw relative to the much larger ones at the fracture origin. These smaller ones (Fig. 2a) were simply intercepted by the propagating crack. Polished surfaces also revealed the polycrystalline ZrO_2 inclusions partially surrounded by their crack-like void, as shown in Fig. 2b.

It is obvious from previous work[3] that the crack-like voids associated with the polycrystalline ZrO_2 inclusions were produced by the differential sintering of a ZrO_2 powder agglomerate within a composite Al_2O_3/ZrO_2 consolidated powder compact. Since the initial ZrO_2 powder contained many large, hard agglomerates, it is also obvious that some were not broken down during milling and ended up in the relatively uniform Al_2O_3/ZrO_2 consolidated compact.

The source of the milling problem appears to be caused by a less than optimum powder plus liquid charge, resulting in an inefficient milling operation. Namely, the same powder plus liquid charge was used here and in the previous work,[2] but the volume of the mill used here was 4 times larger than used in the previous work.[2] In hindsight, the reader may argue the obvious nature of such an error and its strength degrading results. But in learning from such errors, the authors were intent on cataloging these observations to give others improved foresight.

Acknowledgements

This work was supported by the Air Force Office of Scientific Research, Contract No. F49620-81-C-0036.

SC82-16788

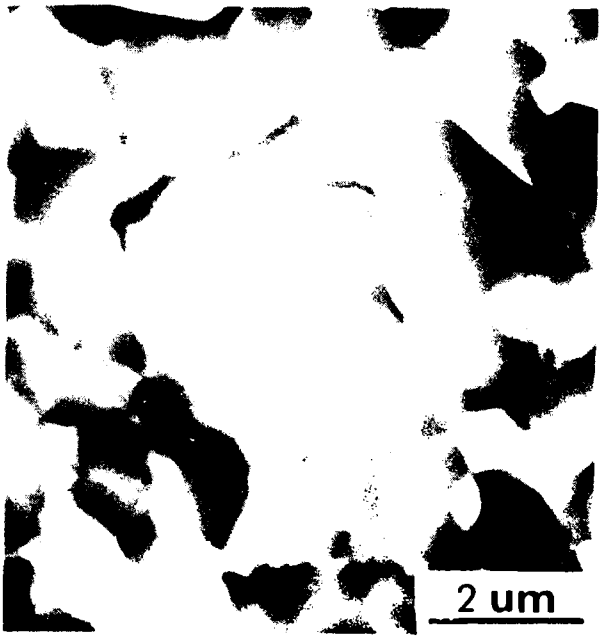

Fig. 2a ZrO_2 inclusion resulting from differential sintering intercepted by crack.

SC82-16789

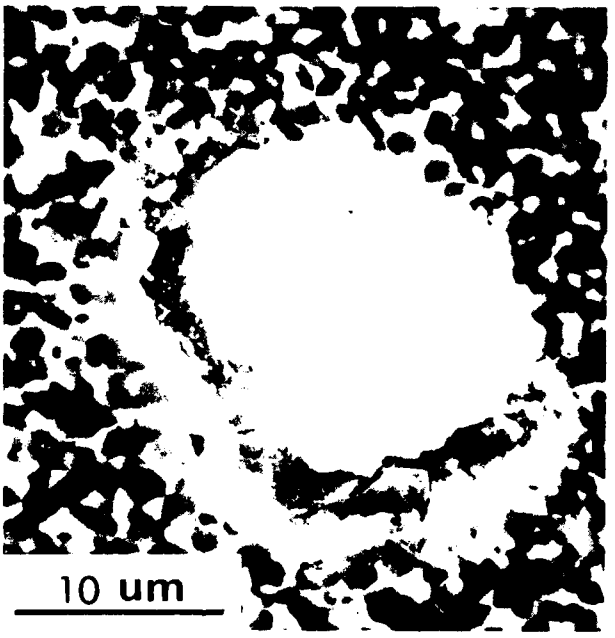

Fig. 2b Crack-like void produced by differential sintering of ZrO_2 agglomerate.

References

1. F.F. Lange, "Processing Related Fracture Origins: Part 1, Observations in Sintered and HIP-Treated Al_2O_3/ZrO_2 Composites," (to be published).

2. I.A. Aksay, B.I. Davis and F.F. Lange," Development of Uniformity in Al_2O_3/ZrO_2 Composites by Colloidal/Filtration Route," (to be published).

3. F.F. Lange and M. Metcalf, "Processing Related Fracture Origins: Part 2, Agglomerate Mobility and Crack-Like Internal Surfaces Caused by Differential Sintering," (to be published).